

See discussions, stats, and author profiles for this publication at: <https://www.researchgate.net/publication/317727008>

Exploring the effect of end-binding proteins and microtubule targeting chemotherapy drugs on microtubule dynamic...

Article in *Journal of Theoretical Biology* · June 2017

DOI: 10.1016/j.jtbi.2017.06.014

CITATIONS

0

READS

31

3 authors:



Diana White

Clarkson University

8 PUBLICATIONS 8 CITATIONS

SEE PROFILE



Stéphane Honoré

Aix-Marseille Université

79 PUBLICATIONS 1,243 CITATIONS

SEE PROFILE



Florence Hubert

Aix-Marseille Université

63 PUBLICATIONS 831 CITATIONS

SEE PROFILE

Some of the authors of this publication are also working on these related projects:



Spatio-temporal simulation of perfusion images by enhancement of contrast [View project](#)



3D Virtual Liver [View project](#)



Exploring the effect of end-binding proteins and microtubule targeting chemotherapy drugs on microtubule dynamic instability



Diana White^{a,*}, Stéphane Honoré^b, Florence Hubert^c

^a Department of Mathematics, Clarkson University, New York, USA

^b Aix-Marseille Université, INSERM UMR S 911, CRO2, Marseille, France

^c Aix-Marseille Université, Institut de Mathématiques de Marseille (I2M), UMR 7373, France

ARTICLE INFO

Article history:

Received 11 December 2016

Revised 17 May 2017

Accepted 13 June 2017

Available online 20 June 2017

Keywords:

Microtubules

Dynamic instability

EBs

MTAs

ABSTRACT

Microtubules (MTs) play a key role in normal cell development and are a primary target for many cancer chemotherapy MT targeting agents (MTAs). As such, understanding MT dynamics in the presence of such agents, as well as other proteins that alter MT dynamics, is extremely important.

In general, MTs grow relatively slowly and shorten very fast (almost instantaneously), an event referred to as a catastrophe. These dynamics, referred to as *dynamic instability*, have been studied in both experimental and theoretical settings. In the presence of MTAs, it is well known that such agents work by suppressing MT dynamics, either by promoting MT polymerization or promoting MT depolymerization. However, recent in vitro experiments show that in the presence of end-binding proteins (EBs), low doses of MTAs can increase MT dynamic instability, rather than suppress it.

Here, we develop a novel mathematical model, to describe MT and EB dynamics, something which has not been done in a theoretical setting. Our MT model is based on previous modeling efforts, and consists of a pair of partial differential equations to describe length distributions for growing and shortening MT populations, and an ordinary differential equation (ODE) system to describe the time evolution for concentrations of GTP- and GDP-bound tubulin. A new extension of our approach is the use of an integral term, rather than an advection term, to describe very fast MT shortening events. Further, we introduce an ODE system to describe the binding and unbinding of EBs with MTs.

To compare simulation results with experiment, we define novel mathematical expressions for time- and distance-based catastrophe frequencies. These quantities help to define MT dynamics in in vivo and in vitro settings. Simulation results show that increasing concentrations of EBs work to increase time-based catastrophe while distance-based catastrophe is less affected by changes in EB concentration, a result that is consistent with experiment.

We further describe how EBs and MTAs alter MT dynamics. In the context of this modeling framework, we show that it is likely that MTAs and EBs do not work independently from one another. Thus, we propose a mechanism for how EBs can work synergistically with MTAs to promote MT dynamic instability at low MTA dose.

Published by Elsevier Ltd.

1. Introduction

Microtubules (MTs) are dynamic protein polymers found in all eukaryotic cells. They are crucial for normal cell development, playing key roles in many cellular processes including cell division, cell polarization, cell motility (Wade, 2009), and cell differentiation (Lacroix and Maddox, 2014). During cell division, MTs help provide the force required to pull two daughter cells apart, and help to properly segregate a cell's genetic material (Wollman et al., 2005).

During cell movement, MT network polarity helps to control the spatial and temporal coordination of migration events, contributing to persistent directed cell migration (Etienne-Manneville, 2013).

MTs are polarized polymers composed of α/β -tubulin heterodimers (Wade, 2009). In most animal cells, MTs grow from the centrosome of the cell, where they are nucleated and capped at their minus end (the end where the majority of α -tubulin is exposed). While their minus end is static, their plus end (the end where the majority of the β -tubulin is exposed), is very dynamic and grows through the addition of guanosine triphosphate (GTP)-bound tubulin dimers. GTP hydrolysis and phosphate release at the growing plus end of the MT lead to the formation of a distinct

* Corresponding author.

E-mail address: dtwhite@clarkson.edu (D. White).

guanosine diphosphate (GDP) region at the back of a growing MT (Desai and Mitchison, 1997) and a stabilizing GTP region at the growing front.

If hydrolysis catches up with the growing front, the stabilizing GTP region is lost and the MT quickly depolymerizes, an event referred to as *catastrophe* (Desai and Mitchison, 1997). As a MT shortens, it is possible for the MT to switch back into a state of growing, an event referred to as *rescue*. The combined dynamics of slow growth and extremely fast depolymerization are referred to as *dynamic instability*, and is unique to MTs.

MTs are one of the primary targets for a large number of cancer chemotherapy drugs (Zhou and Giannakakou, 2005). The reason for this is because they play a key role in cell division and cell motility, and are large structures. Chemotherapy drugs that target MTs belong to a class of MT targeting agents (MTAs) whose primary role is to disrupt cell division and/or proliferation by altering MT dynamics. MTAs can be natural or synthetic, and alter the dynamics of MTs by preventing (MT stabilizing drugs) or promoting (MT destabilizing drugs) (Mukhtar et al., 2014) MT disassembly. The most common MTAs used in the treatment of cancers are those that bind to the vinca, colchicine, and taxane sites along MTs (Mukhtar et al., 2014). Drugs that bind to the vinca and colchicine sites (examples include vinblastine and vincristine) promote MT disassembly, while those that bind to the taxane site (examples include paclitaxel and patupilone) prevent disassembly. At clinically relevant doses, many of these drugs have been found to alter MT dynamics without significantly altering the total MT polymer mass (Zhou and Giannakakou, 2005).

Recent experiments have shown that a certain class of plus-end binding proteins may alter the effect of MTAs on MT dynamics. These proteins, referred to as end-binding proteins (EBs), are part of the +TIP family of proteins that have been found to interact with the growing plus ends of MTs through recognition of the nucleotide state of tubulin at the front end of a growing MT (Jiang and Akhmanova, 2011; Maurer et al., 2012; Zanic et al., 2009). In the presence of EBs, the action of high doses of MTAs on MT dynamics remains relatively unchanged. In particular, MTs polymerize in the presence of stabilizing drugs and depolymerize in the presence of destabilizing drugs. However, at low MTA doses, the dynamics of MTs vary depending on whether or not EBs are present, and the extent to which they are present. In particular, it has recently been discovered that EBs sensitize MTs to the action of MTAs at low MTA doses (Mohan et al., 2013), by promoting rather than suppressing MT dynamic instability.

Over the past few decades, since the discovery of MT dynamic instability (Mitchison and Kirschner, 1984), many mathematical and computational studies have been developed to better understand this dynamical process (Chen and Hill, 1985; Dogterom and Leibler, 1993; Flyvbjerg et al., 1994, 1996; Hinow et al., 2009; Martin et al., 1993; Mishra et al., 2005). Most computational models are designed to study MTs at the microscopic level, taking into consideration the addition and subtraction of individual tubulin dimers (Chen and Hill, 1985; Flyvbjerg et al., 1994, 1996; Martin et al., 1993). Deterministic models have been developed to understand this process at a macroscopic level (Dogterom and Leibler, 1993; Hinow et al., 2009; Mishra et al., 2005). Such models are used to describe the time evolution of length distributions for growing and shortening MT populations. A recent stochastic model has been developed to study the effects of certain MT associated proteins (MAPs) and MTAs on MT dynamics (Hinow et al., 2011). However, to our knowledge, no other theoretical model has been developed to study how EBs alter MT dynamics. In order to understand the possible synergistic effects that MTAs might have on EBs, we first require a detailed understanding of EB/MT dynamics.

We first present a model for MT dynamic instability. This model is an extension of the work by Hinow et al. (2009). Similar to the

approach of Hinow et al. (2009), we use a system of partial differential equations (PDEs) to describe the evolution of growing and shortening MT populations, as well as a coupled system of ordinary differential equations (ODEs) to describe the time evolution of free GTP- and GDP-tubulin. This modeling approach is unique from other models since it describes both variations in total MT length and MT GTP-cap length. Describing the GTP-cap region of a MT is crucial to our approach, since it is at this location that EBs interact with MTs (Jiang and Akhmanova, 2011; Maurer et al., 2012; Zanic et al., 2009). Unlike the model of Hinow et al., we choose a piece-wise continuous growth function, based on experimental evidence, to describe the MT growth rate. Further we choose not to use an advection-type process to describe MT shortening. Instead, we describe MT shortening using an integral term to account for “instantaneous” shortening events of a given size. This is an important consideration, since MTs shorten extremely fast (relative to growth), where their shortening distances can vary according to experimental conditions. To highlight the difference between our new extension and the model of Hinow et al. (2009), we include a number of comparative simulations in the supplementary material.

Next, we develop a modeling framework to describe how EBs work to regulate MT dynamics. To describe the dynamics of EBs, we use a binding/unbinding ODE model, and assume that the primary effect of EBs on MTs is to increase the MT hydrolysis rate, as well as the rescue rate. We assume this since recent experimental studies have shown that the addition of EBs works to increase the time-based frequencies of catastrophe and rescue *in vitro* (Gardner et al., 2011; Vitre et al., 2008). A possible mechanism for the increase in catastrophe frequency is related to the EBs effect on the hydrolysis rate. In particular, some experiments show that the increase in catastrophe rate is correlated to an increase in the hydrolysis rate *in vitro*. Gardner et al. (2011); Maurer et al. (2014). In this study, we restrict ourselves to the study of EBs *in vitro* and leave the study of *in vivo* EB dynamics to our future work.

Finally, we explore the action of MTAs on MTs in the presence and absence of EBs. In the absence of EBs, we assume that the addition of MTAs works through alteration of model parameters directly linked to MT polymerization or depolymerization. By incorporating EB dynamics, we determine that EBs and MTAs do not work independently from one another at low MTA dose, in the context of our modeling framework. As such, we propose a mechanism for how MTAs and EBs can work in a synergistic fashion to promote MT dynamics at low MTA dose.

2. The model

We separate our modeling efforts into three portions. First, in Section 2.1, we describe a new model for MT dynamic instability, which is an extension of the model by Hinow et al. (2009). Here, we introduce a new non-local term to describe MT shortening, as well as a more realistic description for MT growth. Next, in Section 2.2, we describe a method for introducing EBs into the model. Finally, in Section 2.3, we describe a novel method for defining time- and distance-based catastrophe frequencies.

2.1. Modeling MT dynamic instability

Many theoretical models that have been developed to describe the densities of growing and shortening MT populations describe only the time evolution of MT length. In our model, we also take into account the length of the MT cap, which represents the binding region for EBs. In particular, we keep track of the length of the GTP-tubulin zone located at the front end of a growing MT. A similar modeling approach has been used by Hinow et al. (2009). However, unlike the model of Hinow et al., we take into account the action of EBs on MT dynamics. Further, we introduce a novel

description for MT shortening which takes into account fast shortening events of variable size. In particular, our approach provides a new description for MT catastrophe.

In addition to our new description for MT catastrophe, we also derive expressions for time- and distance-based catastrophe. These expressions are crucial to the modeling process, since they allow us to compare our simulation results with experiment.

Here, $u(x, z, t) > 0$ describes the density of growing MTs of length $x > 0$, cap size $z > 0$, at time $t > 0$, while $v(x, t) > 0$ describes the density of shrinking MTs of length x at time t . The variables $p(t)$ and $q(t)$ are the concentrations of free GTP-tubulin and GDP-tubulin at time t , respectively.

2.1.1. A model for growing MTs

Eq. (1) describes the evolution of growing MTs.

$$\begin{aligned} \frac{\partial u(x, z, t)}{\partial t} + \gamma^{poly}(p(t)) \frac{\partial u(x, z, t)}{\partial x} \\ + (\gamma^{poly}(p(t)) - \gamma^h) \frac{\partial u(x, z, t)}{\partial z} = 0 \end{aligned} \quad (1)$$

The second term of Eq. (1) describes MT growth with growth rate $\gamma^{poly}(p(t))$. In most MT dynamic models, the MT growth rate is either taken to be constant (Dogterom and Leibler, 1993) or linearly dependent on free GTP-tubulin concentration (Hinow et al., 2009). Here, we describe a piece-wise linear MT growth rate in terms of experimental observations. In particular, MTs undergo periods of growth that are dependent on the free GTP-tubulin concentration. An example of $\gamma^{poly}(p(t))$, which is similar to growth curves found in experiment (Lodish et al., 2000; Wicczorek et al., 2015) is given by Eq. (2).

$$\gamma^{poly}(p(t)) = \begin{cases} 0 & \text{when } p < p_c \\ \alpha(p(t) - p_c) & \text{when } p_s > p > p_c \\ \alpha(p_s - p_c) & \text{when } p > p_s \end{cases} \quad (2)$$

Here, p_c represents the tubulin concentration required to initiate MT growth, and is called the critical tubulin concentration. The parameter p_s represents the concentration at which the growth rate saturates.

The third term in Eq. (1) describes the rate of change of the MT cap. Here, the cap size varies at a rate equal to the difference between a constant hydrolysis rate γ^h and the growth rate $\gamma^{poly}(p(t))$. We denote this difference as $R(t) = \gamma^{poly}(p(t)) - \gamma^h$ and say

if $R(t) > 0$, the MT cap is growing in length, and
if $R(t) < 0$, the MT cap is shortening in length.

New MTs are nucleated (created) according to the boundary condition (3),

$$\gamma^h u(x, x, t) = \frac{N(p)\xi(x)}{L^*} \quad (3)$$

with

$$N(p) = \mu p^n H(p, p_N). \quad (4)$$

In vitro experiments highlight the fact that, below a certain free tubulin concentration, MT nucleation no longer persists. To represent this in our model, we define $H(p, p_N)$ as a smooth approximation to the heavy-side function such that

$$H(p, p_N) = \frac{1}{2} (1 + \tanh(c(p - p_N))). \quad (5)$$

This function is used to describe a nucleation switch. Specifically, if the GTP-tubulin concentration falls below a critical nucleation value p_N , nucleation is switched off. The parameter c can vary, where higher values correspond to a sharper switch (here $10 < c < 100$). The parameter μ is a constant and is referred to as the nucleation parameter (Hinow et al., 2009), n is the minimum number

of GTP-tubulin dimers required for nucleation, and L^* is the length of freshly nucleated MTs

$$L^* = \int_0^\infty \xi(x) x dx. \quad (6)$$

The parameter $\xi(x)$ describes the length distribution of newly formed MTs. Newly formed MTs generally only consist of a very small number of dimers (Sept et al., 1999), thus we also choose $\xi(x)$ to be an approximation of the heavy side function defined for small x ,

$$\xi(x) = 1 - H(x, x_{max}). \quad (7)$$

Here, x_{max} describes the largest length of a freshly nucleated MT. Typically this value is very small (see Table 1).

If $R(t) > 0$, the MT cap is in a state of growing and MTs in the shrinking state are rescued at a constant rate λ . These MTs can enter back into the growing class of MTs according to the boundary condition (8).

$$R(t)u(x, 0, t) = \lambda v(x, t), \text{ for } R(t) > 0 \quad (8)$$

2.1.2. A novel approach for modeling MT shortening

Eq. (9) describes the evolution of shrinking MTs.

$$\begin{aligned} \frac{\partial v(x, t)}{\partial t} = -\delta \left(\int_0^x k(x, \tilde{x}) v(x, t) d\tilde{x} - \int_x^\infty k(\tilde{x}, x) v(\tilde{x}, t) d\tilde{x} \right) \\ - \begin{cases} \lambda v(x, t) & \text{if } R(t) > 0 \\ R(t)u(x, 0, t) & \text{if } R(t) < 0 \end{cases} \end{aligned} \quad (9)$$

The rightmost terms describe how MTs enter and exit the shrinking state. In particular, MTs can exit this state at a rate λ if $R(t) > 0$ (i.e., if a rescue occurs) and enter back into the growing state according to the boundary condition (8). If $R(t) < 0$, MTs in a growing state with a cap size $z = 0$ enter back into the shrinking state. Once in the shrinking state, MTs shorten according to the first two terms in Eq. (9). The first term in Eq. (9) describes MTs that shorten from length x to some smaller length, while the second term corresponds to MTs that shorten to x from some larger length. The rate of shortening is given by the parameter δ , and the probability that a shortening event of a particular size will occur is defined by the shortening kernel k .

When a MT undergoes a shortening event, it may completely depolymerize or it may only partially depolymerize. Here, we consider the case of a partial shortening event, and leave the case of full depolymerization to a later study. To model full depolymerization, one could simply remove the shortening state completely, and incorporate the shortening kernels into the equation for growing MTs. However, the shortening state, which involves rescue, is a crucial component of our description for time- and distance-based catastrophe (as explained in Section 2.3). In the case of partial shortening, a MT that undergoes a catastrophe (a switch from growth to shortening) shortens by a certain length x_0 . In the experiments that we compare our simulation results to, this length ranges between 1 to 6 μm (Pagano et al., 2012). Fig. 1(a) shows an example of four kymographs, each showing the growth trajectory of a single MT *in vitro* (Pagano et al., 2012). Reading from top to bottom, we see that each MT grows at a relatively constant rate, while undergoing a number of shortening events (each followed by rescue).

Using data collected from a large number of kymographs, like those illustrated in Fig. 1(a), one can determine the mean shortening distance x_0 , as well as its' standard deviation SD. An appropriate shortening kernel k that describes a shortening event from some length x to a smaller length \tilde{x} is the Gaussian distribution centered at $x - x_0$. That is,

$$k(x, \tilde{x}) = \frac{1}{\sigma\sqrt{2\pi}} \exp \frac{-((x - x_0) - \tilde{x})^2}{2\sigma^2}. \quad (10)$$

Table 1
Table of model parameters.

Model parameter	value	source
Growth parameter α	0.1–15 $\frac{\mu\text{m}}{\text{M}\cdot\text{min}}$	Walker et al. (1988)
Critical GTP-tubulin concentration p_c	1–2 μM	Wieczorek et al. (2015), Honore (2015)
Saturation GTP-tubulin concentration p_s	10–12 μM	Honore (2015)
Nucleation critical concentration p_N	12 μM	Honore (2015)
Baseline hydrolysis rate γ^h	1–21 $\frac{\mu\text{m}}{\text{min}}$	Flyvbjerg et al. (1996), [This paper]
Shortening rate δ	5–25 $\frac{\mu\text{m}}{\text{min}}$	Walker et al. (1988), [This paper]
Mean shortening distance x_0	2–6 μm	Walker et al. (1988), [This paper]
Standard deviation of shortening distance SD	0.5–1 μm	Walker et al. (1988), [This paper]
Rescue propensity λ	0.136 $\frac{1}{\text{min}}$	Hinow et al. (2009)
Nucleation rate μ	$10 \times 5.9 \times 10^3 \frac{\text{M}}{\text{min}}$	Hinow et al. (2009)
Dimer nucleation number n	1–12	Sept et al. (1999)
Max length of freshly nucleated MT x_{max}	0.5 μm	[This paper]
GDP/GTP-tubulin exchange rate κ	3–120 $\frac{1}{\text{min}}$	Sept et al. (1999)

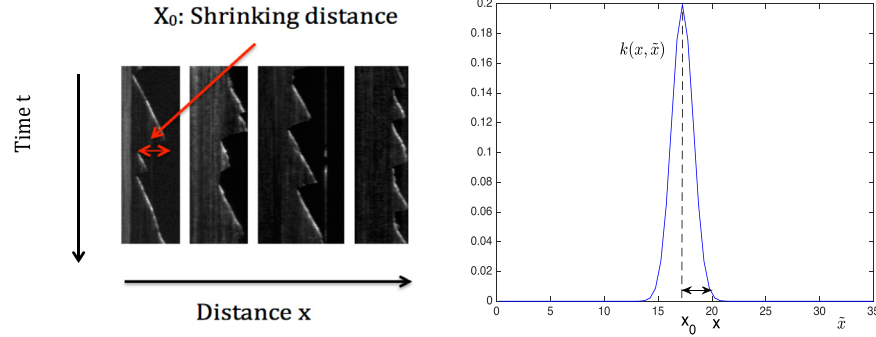


Fig. 1. (a) Kymographs of four MTs that do not completely shrink when they undergo a catastrophe event (MTs are rescued). These results are taken from the EB tip tracking assay in Pagano et al. (2012). Here, EBs were labeled using green fluorescent proteins (GFP), and experiments were carried out with 75 nM EB and 15 μM tubulin. Observations were completed using TIRF microscopy. (b) Example of the shortening kernel k that can be used to describe this type of shortening event. Here, a MT of length x is most likely to shorten by length x_0 . (For interpretation of the references to colour in this figure legend, the reader is referred to the web version of this article.)

2.1.3. Equations for free GTP-tubulin and free GDP-tubulin

Next, we state the equations for the time evolution of free GTP- and free GDP-tubulin concentrations, denoted by $p(t)$ and $q(t)$, respectively.

$$\frac{dp}{dt} = -\gamma^p(p(t)) \int_0^\infty \int_0^x u(x, z, t) dz dx - \mu p^n + \kappa q \quad (11)$$

$$\frac{dq}{dt} = \delta \int_0^\infty x \left(\int_0^x k(x, \bar{x}) v(x, t) x d\bar{x} - \int_x^\infty k(\bar{x}, x) v(\bar{x}, t) \bar{x} d\bar{x} \right) dx - \kappa q \quad (12)$$

The first term on the right-hand side of Eq. (11) describes the uptake of GTP-tubulin as a MT grows, while the second term describes GTP-tubulin used in the nucleation process. The final term is added to describe the exchange of GDP-tubulin to GTP-tubulin (where κ describes this exchange rate). Finally, the first term in Eq. (12) describes all GDP-tubulin that comes from a shortening event while the second term describes GDP/GTP exchange. As a simplifying assumption, we assume that there is a constant supply of chemical energy, so that the GDP/GTP recycling rate κ remains fixed for the entirety of each simulation. Further, we assume that free tubulin diffusion is much faster than the rate at which tubulin is incorporated back into a growing MT (thus, tubulin is distributed homogeneously throughout the domain). In future studies, it would be interesting to test the extent to which diffusion of tubulin alters the MT dynamic results determined in this paper.

All the terms (except those describing GDP/GTP exchange) from Eqs. (11) and (12) come from a conservation property, as described in detail in Hinow et al. (2009). In particular, for conservation of

Table 2

Table of model variables and functions.

Model variable/function	meaning
$u(x, z, t)$	Growing MTs with length x , cap size z , at time t .
$v(x, t)$	Shortening MTs with length x , at time t .
$p(t)$	GTP-tubulin concentration
$q(t)$	GDP-tubulin concentration
$\gamma^{poly}(p(t))$	Growth rate of MTs
$k(x, \bar{x})$	Probability of shortening event from length x to \bar{x}
$\xi(x)$	Length distribution of nucleated MTs.

tubulin in polymer and free form we require that

$$\frac{d}{dt} (u_{tot}(t) + v_{tot}(t) + p(t) + q(t)) = 0, \quad (13)$$

where

$$u_{tot}(t) = \int_0^\infty \int_0^x u(x, z, t) x dz dx = \text{total tubulin in growing MTs} \quad (14)$$

and

$$v_{tot}(t) = \int_0^\infty v(x, t) x dx = \text{total tubulin in shrinking MTs.} \quad (15)$$

All model parameters, functions, and variables for the model described above are summarized in Tables 1 and 2.

2.2. A model for EB dynamics

EBs form comet-like accumulations at the growing ends of MTs. Evidence supports the fact the EBs recognize the nucleotide state of the MT, distinguishing between newly added GTP-tubulin

and hydrolyzed GDP-tubulin (Jiang and Akhmanova, 2011; Maurer et al., 2012; Zanic et al., 2009). EBs do not track the end of growing MTs processively, but rather exchange very rapidly between bound and unbound states (Jiang and Akhmanova, 2011). Binding and unbinding rates can vary, depending on experimental conditions. Such conditions include the amount of EB present in the system and the availability of binding sites along the GTP cap (Maurer et al., 2014).

EBs alter MT dynamics in many ways. Some *in vitro* studies show that increasing concentrations of EBs work by increasing both the catastrophe and rescue frequency of MTs (Maurer et al., 2014; Vitre et al., 2008). Further, these studies show that EBs also increase the MT growth rate in a concentration dependent way (Maurer et al., 2014).

We model EB dynamics by a binding/unbinding process, where the unbinding rate is constant (Maurer et al., 2012) and the binding rate depends on the size of the GTP-tubulin cap region (i.e., the amount of GTP-tubulin in a growing MT). This assumption is based on experimental evidence that suggests that EB binding is dependent on the availability of binding sites, where we assume that the number of binding sites is directly proportional to the size of the GTP cap. Eqs. (16) and (17) describe the time evolution of bound, $EB^b(t)$, and unbound, $EB^u(t)$, EB populations:

$$\frac{dEB^b(t)}{dt} = k_{on}(u_{cap}(t))EB^u(t) - k_{off}EB^b(t) \quad (16)$$

$$\frac{dEB^u(t)}{dt} = -k_{on}(u_{cap}(t))EB^u(t) + k_{off}EB^b(t), \quad (17)$$

where $EB^b(t) + EB^u(t)$ is constant. Here, k_{off} describes the constant rate of EB detachment and the function $k_{on}(u_{cap}(t))$ describes the rate at which EBs bind to the MT cap. As stated before, this rate is dependent on the amount of GTP-tubulin (p) in the cap region of the MT, which we will call $u_{cap}(t)$. Here, we define the total amount of tubulin in the cap as

$$u_{cap}(t) = \int_0^\infty \int_0^x u(x, z, t) dz dx \quad (18)$$

and choose $k_{on}(u_{cap}(t))$ such that

$$k_{on}(u_{cap}(t)) = k_{on}^{max} u_{cap}(t), \quad (19)$$

where k_{on}^{max} is the maximum attachment rate for EBs. It is well known that the distribution of EBs along the cap region is not uniform, but varies, producing EB comets (Maurer et al., 2014). However, as a first approximation we consider the case where EBs bind uniformly along the entire length of the GTP cap region.

As stated above, recent *in vitro* studies show that EBs work to increase both the catastrophe and rescue frequencies, as well as the growth rate of MTs (Maurer et al., 2014). One theory for EBs influence on the catastrophe frequency is that EBs act by increasing the hydrolysis rate, which in turn increases the catastrophe frequency (Gardner et al., 2011; Maurer et al., 2014).

Here, we assume that bound EBs increase the rate of hydrolysis γ^h in a density dependent way. In particular, instead of considering a constant hydrolysis rate γ^h (as described in Eq. (1)), we consider an EB dependent hydrolysis rate

$$\gamma_{EB}^h(t) = \gamma^h + f_1(EB^b(t)), \quad (20)$$

where γ^h describes the original hydrolysis rate given in Table 1, and $f_1(EB^b(t))$ describes the increase in hydrolysis from baseline due to the addition of bound EBs (i.e., we define $f_1(EB^b(t))$ to be a monotonically increasing function with respect to bound EBs). We also include the action of EBs on the rescue rate λ . In particular, we assume that EBs increase the rescue rate in a similar density dependent way.

$$\lambda_{EB}(t) = \lambda + f_2(EB^b(t)) \quad (21)$$

Table 3
Table of EB model parameters.

Model parameter	value	source
Detachment rate of EB k_{off}	$30 \frac{1}{\text{min}}$	Maurer et al. (2014)
Max attachment rate of EB k_{on}^{max}	$15 \frac{1}{\mu M \cdot \text{min}}$	[This paper]
EB hydrolysis constant γ_{EB}^h	$50 \frac{1}{\mu M}$	[This paper]
EB rescue constant λ_{EB}	$20 \frac{1}{\mu M}$	[This paper]

It is possible that EBs increase the rescue frequency of MTs by binding along their entire length, and not just to their cap region. In particular, it has been observed that at moderate to high concentrations of EBs, EBs can bind along the entire length of a MT, protecting MTs from depolymerization (Honore, 2015).

As a first assumption, we define a linear response of EBs to hydrolysis and rescue so that $f_1(EB^b(t)) = \gamma_{EB}^h EB^b(t)$ and $f_2(EB^b(t)) = \lambda_{EB} EB^b(t)$, where γ_{EB}^h and λ_{EB} are positive constants that we refer to as the EB hydrolysis constant and the EB rescue constant, respectively. All EB model parameters are summarized in Table 3, where the choice of γ_{EB}^h and λ_{EB} are explained later in the Numerical Details Section.

2.3. Defining time- and distance-based catastrophe frequency

In this section, we derive mathematical expressions for time- and distance-based catastrophe frequency. These are two of the key quantities that help to define MT dynamic instability *in vitro* and *in vivo*. Thus, they can be used to compare simulation results with experiment. Other quantities of interest that help to describe MT dynamics include the mean MT growth rate, the MT cap size, and the EB decoration time (DT). MT cap size is defined by Eq. (18), and we will define mean MT growth rate and DT at the end of this section.

Time-based catastrophe (for a single MT) is defined as the number of catastrophe events divided by the total time a MT spends growing (Walker et al., 1988). In our model, we describe the dynamics of a population of MTs, where many catastrophe events can occur at a single instant in time (such catastrophes occur when $R(t) < 0$ and the MT cap size is $z = 0$).

The expression $\int_0^\infty u(x, 0, t) dx$ corresponds to the total number of MTs with cap size zero at time t . Thus, when $R(t) < 0$, this expression corresponds to the total number of MTs that undergo a catastrophe at time t . In general, $R(t)$ oscillates between values that are positive and negative (i.e., MTs switch between phases of growing and shrinking), and there can be multiple time intervals for which MTs undergo catastrophe events. Here, we define the average time-based MT catastrophe rate as

$$J_c^{time} = \frac{1}{N} \sum_{i=1}^N \frac{\int_{I_i} \frac{1}{T_{grow}(t)} \int_0^\infty u(x, 0, t) dx dt}{\int_{I_i} \int_0^\infty u(x, 0, t) dx dt}, \quad (22)$$

where N denotes the number of time intervals for which $R(t) < 0$, I_i corresponds to an interval of time for which $R(t) < 0$, and $T_{grow}(t)$ corresponds to the time between a catastrophe event and the time a MT begins to grow. A MT starts to grow after a rescue, or it has been growing since it was nucleated. For simplicity, we approximate the latter as the time when nucleation ends (i.e., when $p_N \leq 12 \mu M$). At this time, the number of MTs in the system, $\int_0^\infty \int_0^x u(x, z, t) dz dx$, remains constant (this can be shown by integrating Eq. (1) over x and z).

To understand the formulation of Eq. (22), consider Fig. 2, which illustrates an example of an oscillating $R(t)$. Here, there are three time intervals corresponding to $R(t) < 0$. Specifically, $I_1 = [t_0, t_1]$, $I_2 = [t_2, t_3]$, and $I_3 = [t_4, t_5]$. The red line corresponds to the time t^* when the nucleation process stops.

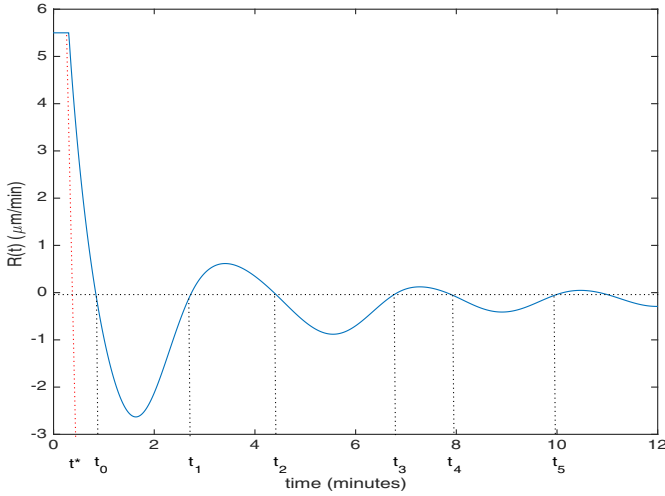


Fig. 2. Example of the time evolution of $R(t)$. If $R(t) > 0$, a MT can be rescued and its' cap grows. If $R(t) < 0$, a MTs' cap will shrink and the MT can undergo a catastrophe if it loses its' cap ($z = 0$). Here, there are three time intervals for $R(t) < 0$. Specifically, $I_1 = [t_0, t_1]$, $I_2 = [t_2, t_3]$, and $I_3 = [t_4, t_5]$. The red line corresponds to the time t^* when nucleation stops. (For interpretation of the references to colour in this figure legend, the reader is referred to the web version of this article.)

If a catastrophe occurs during the first time interval $I_1 = [t_0, t_1]$, the growing time $T_{grow}(t)$ is simply the time between the catastrophe event and the time t^* . However, if a catastrophe occurs during a later time interval, we must determine whether the MT came from a previous rescue event, or if it came from t^* .

To determine $T_{grow}(t)$, we make use of the method of characteristics. In particular, we consider the Eq. (1) for growing MTs. This equation is of the hyperbolic type, where the characteristic equations for $x(t)$ and $z(t)$ are given by

$$\frac{dx}{dt} = \gamma^{poly}(p(t)) \tag{23}$$

$$\frac{dz}{dt} = \gamma^{poly}(p(t)) - \gamma^h \tag{24}$$

and $u(x(t), z(t), t)$ is constant along these characteristics. By solving the equations, using initial conditions $x(0) = x_0$ and $z(0) = z_0$, we obtain

$$x(t) = x_0 + \int_{t_0}^t \gamma^{poly}(p(s)) ds \tag{25}$$

$$z(t) = z_0 + \int_{t_0}^t R(s) ds, \tag{26}$$

since $R(t) = \gamma^{poly}(p(t)) - \gamma^h$. As an example, let us consider catastrophe events that occur during the second time interval $I_2 = [t_2, t_3]$ when $R(t) < 0$. In particular, let us consider a time \bar{t} between t_2 and t_3 at which a population of MTs undergo a catastrophe so that $z(\bar{t}) = 0$ (the MT cap size is zero, and MTs enter the shrinking state). To determine the growing (existence) time of the density of MTs $u(x(\bar{t}), 0, \bar{t})$, it suffices to trace back along the characteristic to a time \hat{t} such that $z(\hat{t}) = 0$ for $R(t) > 0$ (this time corresponds to a birth/rescue event). In this case, Eq. (26) becomes

$$z(\bar{t}) = z(\hat{t}) + \int_{\hat{t}}^{\bar{t}} R(s) ds$$

$$0 = \int_{\hat{t}}^{\bar{t}} R(s) ds$$

$$0 = \int_{\hat{t}}^{t_0} R(s) ds + \int_{t_0}^{\bar{t}} R(s) ds.$$

For the example given in Fig. 2, there will be a time between t_2 and t_3 after which you can not trace back to the previous time interval to determine a time \hat{t} such that $z(\hat{t}) = 0$. In this case, the existence/growing time is given by the time between the catastrophe event and t^* .

Distance-based catastrophes are defined as the number of catastrophe events divided by the length to which a MT grows before it undergoes a catastrophe (Walker et al., 1988). Here, we define the average distance-based MT catastrophe rate as

$$f_c^{dist} = \frac{1}{N} \sum_{i=1}^N \frac{\int_{\hat{t}_i}^{t_i} \frac{1}{L_{grow}(t)} \int_0^\infty u(x, 0, t) dx dt}{\int_{\hat{t}_i}^{t_i} \int_0^\infty u(x, 0, t) dx dt}, \tag{27}$$

where $L_{grow}(t)$ is the length to which a MT grows before it undergoes a catastrophe. Similar to how we defined the growing time, we can make use of the method of characteristics to determine the growth length $L_{grow}(t)$. In particular, if we consider the example given above, we can write Eq. (25) as

$$x(\bar{t}) = x(\hat{t}) + \int_{\hat{t}}^{\bar{t}} \gamma^{poly}(p(s)) ds.$$

Adding and subtracting γ^h under the integral sign and writing in terms of $R(t)$ we obtain

$$x(\bar{t}) = x(\hat{t}) + \int_{\hat{t}}^{\bar{t}} (R(s) + \gamma^h) ds,$$

which simplifies to

$$x(\bar{t}) = x(\hat{t}) + \int_{\hat{t}}^{\bar{t}} R(s) ds + \gamma^h(\bar{t} - \hat{t})$$

in the case where γ^h is constant. As $\int_{\hat{t}}^{\bar{t}} R(s) ds = 0$, we have

$$x(\bar{t}) - x(\hat{t}) = \gamma^h(\bar{t} - \hat{t}),$$

which is the same as the expression

$$L_{grow}(t) = \gamma^h T_{grow}(t). \tag{28}$$

When EBs are added (and γ^h is not constant), Eq. (28) is given by

$$L_{grow}(t) = \int_{\hat{t}}^{\bar{t}} \gamma_{EB}^h(t) ds. \tag{29}$$

For constant hydrolysis, if we substitute Eq. (28) into (27) we have the relation

$$\gamma^h = \frac{f_c^{time}}{f_c^{dist}}. \tag{30}$$

It is often difficult to calculate the hydrolysis rate directly in experiments. However, a relation similar to (30) has been observed experimentally. In particular, it has been observed that the MT growth rate is approximately equal to the ratio of the time-based catastrophe frequency to the distance-based catastrophe frequency (Pagano et al., 2012). In our model, the hydrolysis rate and the growth rate are always close in value (they oscillate about each other). Thus, the resulting expression (30) is consistent with experiment, and we are confident that the mathematical expressions we derived for the catastrophe frequencies are biologically realistic in the context of our modeling framework.

The mean MT growth rate $\bar{\gamma}^{poly}$ is easily defined using Eq. (2) by taking the average of this expression over some defined period of time. For example,

$$\bar{\gamma}^{poly} = \text{Mean}_{T_{min} < t < T_{max}} (\gamma^{poly} p(t)) \tag{31}$$

is the mean of (2) between T_{min} and T_{max} , where T_{min} is some initial time after which there is no nucleation and T_{max} is the maximum time of simulation.

Table 4
Parameters for the control test.

Parameter	p_c	p_s	α	γ^h	δ	x_0	SD of x_0	λ	μ	n	κ
SI units	μM	μM	$\frac{\mu\text{m}}{\text{min}\cdot\mu\text{M}}$	$\frac{\mu\text{m}}{\text{min}}$	$\frac{\mu\text{m}}{\text{min}}$	μm	μm	$\frac{\mu\text{m}}{\text{min}}$	$\frac{1}{\mu\text{M}\cdot\text{min}}$		$\frac{1}{\text{min}}$
Value	2	12	2	3.8	15	4	1	0.136	59×10^{-4}	2	1

Decoration time is the length of time EB decorates (or is located along) the MT cap, and is calculated experimentally by keeping track of the existence time of EB binding sites using GFP-labeled EBs (Maurer et al., 2014). More specifically, it is the length of the EB zone divided by the growth rate of a MT. In our model, we assume the EBs are distributed uniformly along the cap region, where the length of the EB region at any instant in time is defined by Eq. (18) and DT (as a function of time) is defined by,

$$\text{DT}(t) = \frac{u_{\text{cap}}(t)}{\bar{\gamma}^{\text{poly}}(p(t))}. \quad (32)$$

3. Numerical details

We simulate our model using a finite volume method. For the advection terms in Eq. (1) we use an upwinding approach, while for the ODEs (12) and (11) we use an explicit Euler strategy. All integral terms are calculated using order 0 quadrature methods, adjusted to preserve tubulin at the discrete level.

All simulations are implemented in Matlab using custom code similar to that outlined in Barlukova et al. 2017. We discretize our domain into 200×200 cells, where each cell has a dimension of $0.5\mu\text{m}$ (our domain in $100\mu\text{m} \times 100\mu\text{m}$). Because the MT growth rate and hydrolysis rate change in time, we use an adaptive time step (with a maximum time step of 0.1) to ensure that our scheme satisfies the CFL condition (Zauderer, 2006).

The quantities for GTP and GDP-tubulin (p and q) are measured in μM (1 micromole per liter), and the length of a MT and its' GTP cap region are measured in μm . Similar to Hinow et al. (2009), we define a conversion factor to represent μM in terms of μm , so that all units are consistent. In particular, in $1 \mu\text{mol}$ of tubulin, there are $N_A \times 10^{-6}$ molecules of tubulin, where $N_A = 6.022 \times 10^{23}$ is Avogadro's number. Here, we assume a MT is one-dimensional, where in reality most MTs are composed of 13 protofilaments. Thus, we estimate the length of one dimer in our model, l_{unit} , to be the true length of a dimer divided by 13. That is,

$$l_{\text{unit}} = \frac{8.12 \times 10^{-3}}{13} \mu\text{m}.$$

Thus, the factor of conversion from μM to μm is

$$\text{conv} = 6.022 \times 10^{17} \times l_{\text{unit}}.$$

3.1. Choice of control parameters

The parameter values for λ , n , and κ , are the same as those used in Hinow et al. (2009). The parameter μ is ten times that used in Hinow et al. (2009). The reason for increasing this parameter is that increases only lead to an increase in the nucleation process, while the qualitative results of the solution curves remain unchanged (this is explained in Hinow et al. (2009)). All other model parameters are within realistic experimental range (see Table 1) and are selected so as to give simulated output that is consistent with the experiment of Pagano et al. (2012) (this experiment was completed with 75 nM of EBs). Table 4 provides a summary of these control parameters, which we refer to as our baseline parameter set. Table 5 corresponds to a comparison between the simulated and experimental observables using the baseline parameter set. In particular, it outlines the simulated mean growth rate ($\bar{\gamma}^{\text{poly}}$) and the catastrophe frequencies (f_c^{time} and f_c^{dist}), as

well as the corresponding values calculated from the experiment of Pagano et al. (2012). It can be noted that simulated values are consistent with experiment.

The maximum attachment rate and detachment rate ($k_{\text{on}}^{\text{max}}$ and k_{off}) for EBs, as well as the EB hydrolysis and rescue constants (γ_{EB}^h and λ_{EB}) are given in Table 3. The parameter k_{off} is that which is reported in the study of Maurer et al. (2014), while the other model parameters were selected to obtain simulated outputs that are consistent with the experiment of Pagano et al. (2012) (recall Table 5).

4. Results

We divide our results section into three main parts. First, we incorporate EBs into our model and show how they affect the frequencies of catastrophe f_c^{time} and f_c^{dist} , the mean MT growth rate $\bar{\gamma}^{\text{poly}}$, the mean MT cap length, and the EB decoration time, DT. Next, we describe how variations in specific model parameters affect MT dynamics. We do this to gain insight into which parameter variations promote polymerization and which promote depolymerization, similar to the action of stabilizing and destabilizing MTAs, respectively. In particular, we assume that the action of MTAs is implicit in this model, and that the addition of MTAs work through variation of certain model parameters. We describe which variations are more likely to be biologically relevant, according to what is known about the effect of MTAs on MT dynamics *in vitro*. Finally, we describe a potential mechanism to explain how MTAs work to sensitize the effect of EBs on MT dynamics.

4.1. Effect of EBs on MT dynamics

Fig. 3 illustrates results for total polymerized tubulin in growing and shortening MTs ($u_{\text{tot}}(t)$ and $v_{\text{tot}}(t)$), as well as the free GTP- and GDP-tubulin concentrations over time. Here, we simulate Eqs. (1), (9), (11), and (12), using the control parameter set in Table 4. We choose initial conditions $p(0) = 15\mu\text{M}$, and $q(0) = v(:, 0) = u(:, :, 0) = 0$, as these are the same conditions used in the study of Pagano et al. (2012). Fig. 3(a) and 3(c) illustrate these results in the absence and presence of 75nM EBs, respectively, and Figs. 3(b) and 3(d) describe the corresponding decoration times.

In Fig. 3, the thin solid black line represents the total polymerized tubulin in growing MTs, while the dotted line represents the total polymerized GDP-tubulin in growing MTs. Specifically,

$$\text{total polymerized GDP-tubulin} = \int_0^\infty \int_0^x u(x, z, t)(x - z) dz dx.$$

The distance between both curves represents the MT cap length. In this example, the average cap length decreases over time. From Fig. 3, we note that the average DT decreases for increasing EB concentration. These results are consistent with experiment (Maurer et al., 2014; Pagano et al., 2012). Fig. 4 is the same simulation as in Fig. 3(a), but simulated over a longer period of time. It is interesting to note that, when simulated over a longer period of time, oscillations grow, but appear to stabilize.

Next, we show the effect of increasing EB concentration on f_c^{time} , f_c^{dist} , $\bar{\gamma}^{\text{poly}}$, MT cap length, and DT. These values are summarized in Table 6. The control model parameters used in the following simulations are those given in Tables 3 and 4. Again, these parameters are selected so that the simulation output is consistent with the experimental output of Pagano et al. (2012) in the

Table 5
Comparison of model output with experimental data in the presence of 75 nM of EBs and 15 μM tubulin Pagano et al. (2012).

	$\bar{\gamma}^{poly}$	f_c^{time}	f_c^{dist}
SI units	$\mu\text{m min}^{-1}$	min^{-1}	μm^{-1}
Experimental control (Pagano et al., 2012)	3.87 ± 1.00	1.72 ± 0.12	0.47 ± 0.03
Simulated “control” test	3.83	1.73	0.4164

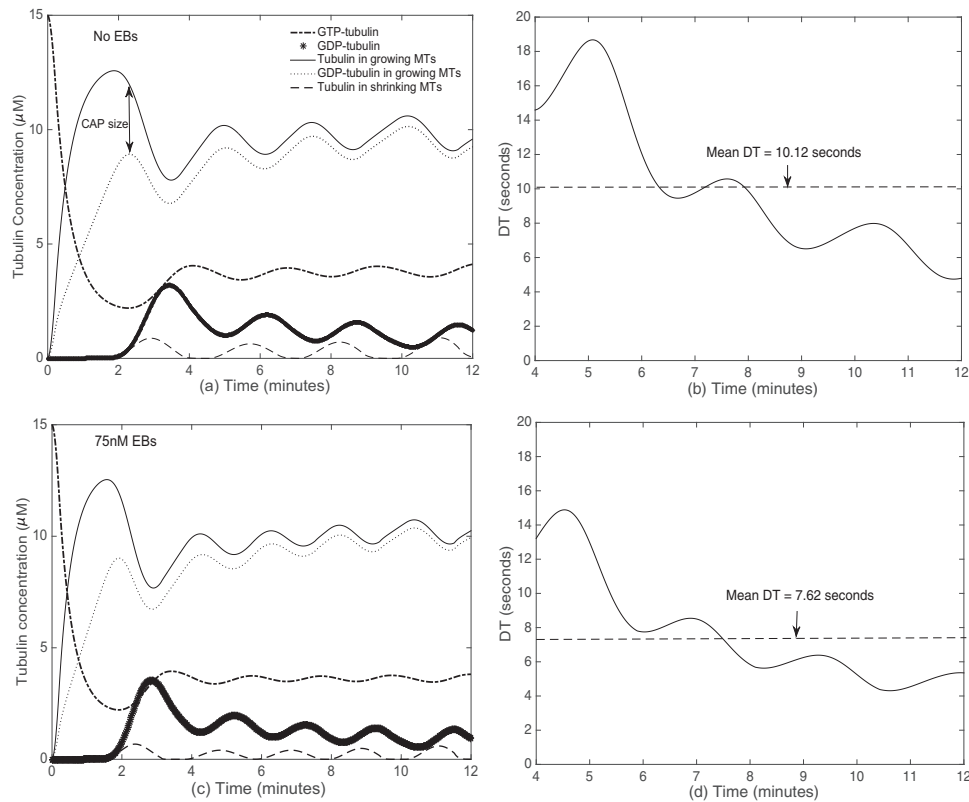


Fig. 3. Oscillating tubulin concentrations and DT. (a) Tubulin concentrations in the absence of EBs, (b) DT in the absence of EBs, (c) tubulin concentrations in the presence of 75 nM EBs, and (d) DT in the presence of 75 nM EBs. Here, our control parameters in Tables 3 and 4 are used.

Table 6
Simulated observables f_c^{time} , f_c^{dist} , $\bar{\gamma}^{poly}$, MT cap length, and DT for increasing EB concentration. EB model parameters are outlined in Table 3.

EB concentration (nM)	0	25	50	75	100	125	150	175
f_c^{time} ($\frac{1}{\text{min}}$)	1.545	1.595	1.686	1.728	1.764	1.730	1.765	1.734
f_c^{dist} ($\frac{1}{\mu\text{m}}$)	0.4077	0.4050	0.4145	0.4164	0.4099	0.3912	0.3898	0.4147
$\bar{\gamma}^{poly}$ ($\frac{\mu\text{m}}{\text{min}}$)	3.54	3.67	3.76	3.83	3.88	3.94	4.00	4.10
MT cap length (μm)	0.59	0.55	0.52	0.49	0.45	0.38	0.40	0.38
DT (sec)	10.12	9.07	8.27	7.62	7.02	6.49	6.02	5.59

presence of 75 nM of EB3. All parameter values fall within experimental range.

From Table 6, we note that there is an increase in the time-based catastrophe frequency for EB concentrations up to 75 nM. Further increases have less effect on changes in the time-based catastrophe frequency. This result is consistent with experiment (Maurer et al., 2014). In particular, it has been observed that at higher values of EB concentration, the time-based catastrophe frequency saturates to some constant value (Maurer et al., 2014). In addition to the time-based catastrophe results, we note that there is little change in the distance-based catastrophe frequency as EB concentration increases, a result that has also been observed experimentally (Maurer et al., 2014; Vitre et al., 2008). From Table 6, we can also note an increase in the mean MT growth rate and a decrease in the DT, for increasing EB concentration. This is a re-

sult that is also consistent with experimental observations (Maurer et al., 2014; Vitre et al., 2008). To determine if our simulated MT cap sizes are realistic, we make comparisons between our results and results from a study in which MT cap sizes were determined in an *in vivo* setting. In particular, Seetapun et al. (Seetapun et al., 2012) suggest that the average cap size *in vivo* for a MT is approximately 700 GTP-tubulin units, corresponding to approximately 50 GTP layers (as there are usually 13 protofilaments that comprise a MT). This length corresponds to a value of 4.14 μm . Further, Seetapun et al. suggest that the cap size *in vitro* should be approximately 7 orders of magnitude smaller in size, as compared to the *in vivo* case. This is due to the fact that the growth rates of MTs *in vivo* are much faster (typically on the order of 7 times faster) than in the *in vitro* case. Reducing the *in vivo* value of 4.14 μm by 7 orders of magnitude results in a cap size of approximately 0.59

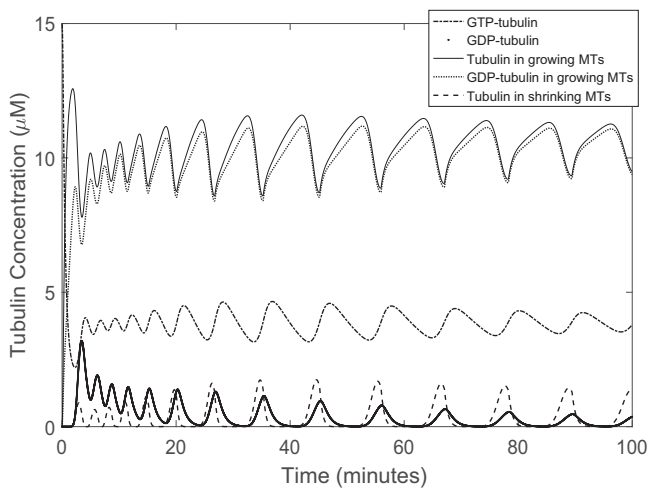


Fig. 4. An extended simulation of Fig. 3(a). The mean MT cap length is 0.43 μm .

μm . This value is the same value we calculated for our control cap size length (see Table 6).

In the case when hydrolysis is constant, we can use the relationships given by equations (28) and (30) to determine the mean length and mean growth time for MTs in the system described in Fig. 3(a). In particular, these values are the reciprocals of their corresponding frequency values. Thus, we find a mean MT length of 2.45 μm , and a mean growing time of 0.65 minutes.

To verify that the results given in Table 6 are not just a result of the baseline parameters selected (parameters from Tables 3 and 4) we include the Appendix A, which gives a summary of results for a range of parameter sets (based on experimental values recorded in Table 1). The results show that for a variety of model parameters, the qualitative results summarized in Table 6 are the same. In Appendix A, we also provide an illustration to explain why these particular trends (increases in time-based catastrophe followed by saturation, and relatively fixed distance-based catastrophes) exist.

4.2. Parameter variation: insight into the action of MTAs on MT dynamics

Here, we describe how changes in certain model parameters affect the behavior of MT dynamics. In particular, in Figs. 5(a), (b), and (c), we show how variations in the MT growth rate parameter α , the GTP/GDP exchange rate κ , and the baseline hydrolysis rate γ^h , change the qualitative behavior of solutions curves that are shown in Fig. 3(a), respectively. Parameter variations are completed in the absence of EBs and our simulations are completed using our control parameter set (parameters given in Table 4). For each figure that follows, we only plot curves for the total polymerized tubulin in growing MTs, unless stated otherwise.

Fig. 5(a) illustrates total tubulin in growing MTs for low and high values of the MT growth rate parameter α . For low values, polymer density is reduced, while for higher values it increases. In particular, for very high values of α , the tubulin concentration in growing MTs is stabilized (i.e., catastrophes are suppressed). This effect is similar to that of a stabilizing drug (like paclitaxel Zhou and Giannakou, 2005), since such drugs increase MT polymerization and stabilization. Thus, it is biologically realistic that the effect of a stabilizing drug, in this modeling framework, is to increase the MT growth rate parameter α .

Fig. 5(b) illustrates MT dynamics for varying GDP/GTP exchange rate κ . Here, we see a similar effect as in Fig. 5(a) (but only for high values of κ). In particular, for high values of κ , the tubulin concentration in growing MTs is stabilized. Although changes in κ

have not been observed experimentally when MT stabilizing drugs are present, our model predicts that this change might exist.

Finally, Fig. 5(c) illustrates the concentration of tubulin in growing MTs for low and high values of the hydrolysis rate γ^h . Here, we see that for low values of this parameter MTs become stabilized, while at higher values MT tubulin mass is decreased. For very high values of γ^h , MTs completely depolymerize. *In vivo* and *in vitro*, MT destabilizers (like vinblastine and vincristine Zhou and Giannakou, 2005) work to depolymerize MTs, decreasing MT polymer mass for increasing dose. Thus, we suggest that the role of MT destabilizing drugs in our model can work by acting to increase the baseline hydrolysis rate γ^h .

A consequence of our modeling approach is that the MT growth rate $\gamma^{poly}(p(t))$ oscillates about the constant hydrolysis rate γ^h (this result is also true for the case when EBs are added and the hydrolysis rate is not constant). Specifically, for a wide variety of parameter choices, MTs undergo periods of growth and shortening, where the MT growth rate is, in a sense, controlled by the value of the hydrolysis rate (i.e., on average the growth rate will be slightly more or slightly less than this value). In the case when α is very small (as shown in Fig. 5(a)), or when γ^h is very large (as shown in Fig. 5(c)), the curves for hydrolysis and MT growth never intersect (see Fig. 6). In this case, MTs will start to grow, but the MT cap will eventually disappear. Once the MT cap size is zero, it will not grow again ($R(t) < 0$ for the rest of time), and so the MT depolymerizes. Thus, for our model, MT destabilizers work to either increase the hydrolysis rate γ^h or to decrease the MT growth rate parameter α (or some combination of these mechanisms). In a recent *in vitro* study, it has been suggested that the primary action of a destabilizing drug (in the absence of EBs) is to decrease the MT growth rate (Mohan et al., 2013). Thus, we suggest that the most biologically realistic action of MT destabilizing drugs is to decrease the MT growth rate parameter α .

Finally, we show results for increasing and decreasing MT shortening rate δ . Initially we suspected that increasing this value would act to depolymerize MTs, however this was not the case. Fig. 7(a) shows that, for values of δ smaller than our baseline value (Fig. 7(b)), oscillations for tubulin in growing MTs increase in size. Also, we see that there is a larger concentration of polymerized tubulin in the shortening MT population. In particular, MTs stay in the shortening phase for a longer period of time. A similar result was also shown in the study of Hinow et al. (2009). Alternatively, if we increase the parameter δ from its' baseline value (Fig. 7(c)), oscillations in the growing MT population decrease from their baseline value, and less MTs are found in the shortening population. A possible explanation for this is that when the MT shortening rate is high, MTs depolymerize more quickly into free GDP-tubulin, which when converted back into free GTP-tubulin promotes MT growth. Qualitatively similar results are found for increases and decreases in the MT shortening length x_0 (i.e., decreasing x_0 has a similar effect as decreasing δ and vice versa - results not shown).

4.3. Exploring the synergistic effect between MTAs and EBs

From the previous section, we showed that increases in both α and κ have a stabilizing effect on MTs, similar to how MT stabilizers (like paclitaxel) work to promote MT polymerization *in vitro* (Zhou and Giannakou, 2005). Further, we showed that reducing the value of the hydrolysis rate γ^h also had a stabilizing effect. In *in vitro* systems that do not comprise of EBs, stabilizing MTAs work to stabilize and promote MT polymerization at most doses (low and high) (Mohan et al., 2013). However, in MT systems where low doses of stabilizing drugs are introduced in the presence of EBs, MTs have been found to oscillate quickly between growing and shortening phases (i.e., MT dynamic instability is promoted) (Mohan et al., 2013; Pagano et al., 2012).

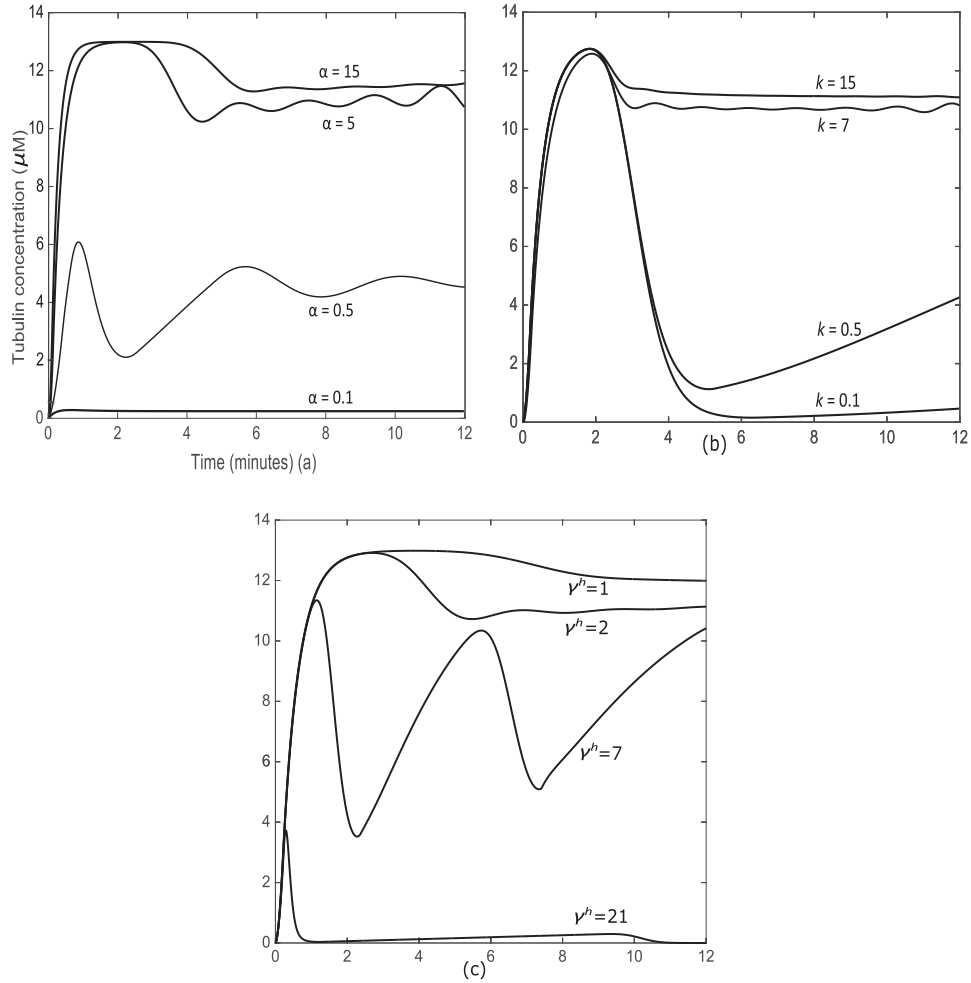


Fig. 5. Change in the total tubulin mass in growing MTs for variations in (a) the growth rate parameter α , (b) the GDP/GTP exchange rate κ , and the (c) hydrolysis rate γ^h . Baseline values are $\alpha = 2.5 \frac{\mu\text{m}}{\mu\text{M}\cdot\text{min}}$, $\kappa = 1 \frac{1}{\text{min}}$ and $\gamma^h = 3.8 \frac{\mu\text{m}}{\mu\text{M}\cdot\text{min}}$.

The promotion of MT dynamic instability in such systems is a recent experimental finding, and the mechanism describing this so called *synergistic effect* between stabilizing MTAs and EBs is not fully understood. Here, we consider two possible mechanisms to describe how low doses of MTAs promote MT dynamic instability in the presence of EBs.

First, we consider the case where the stabilizing drug acts independently from the EBs. Here, we introduce 75 nM of EBs (see Table 3 for EB model parameters) and assume that EBs work by acting on hydrolysis and rescue according to Eqs. (20) and (21) (just as was done before). We further assume that the action of a stabilizing drug is to increase either α or κ (as was described in the previous section).

Figs. 8(a), (b), and (c) show the effect of introducing 75 nM of EBs into a system where stabilizing MTAs are present. Here, we assume $\alpha = 7 \frac{\mu\text{m}}{\mu\text{M}\cdot\text{min}}$ represents a low dose of a stabilizing MTA. In particular, Figure 8(a) illustrates solution curves for $\alpha = 7 \frac{\mu\text{m}}{\mu\text{M}\cdot\text{min}}$ in the absence of EBs, while Fig. 8(b) illustrates the effect of introducing 75 nM EBs into the system. Here, we note that the addition of EBs promote MT oscillations (i.e., EBs promote catastrophe and rescue). Fig. 8(c) illustrates the case where we further increase the MTA dose (an increase to $\alpha = 10 \frac{\mu\text{m}}{\mu\text{M}\cdot\text{min}}$), while the EB concentration remains fixed at 75 nM. Here, we note that the oscillations are smaller than the case when $\alpha = 7 \frac{\mu\text{m}}{\mu\text{M}\cdot\text{min}}$ (i.e., there is a reduction in catastrophe and rescue). We should also note that oscil-

lations are smaller for all values of $7 < \alpha < 10$. In *in vitro* systems, a small increase in the MTA dose should further promote catastrophe and rescue, where it is only at higher MTA doses that catastrophe is suppressed. For example, one study found suppression of MT dynamics at MTA doses greater than 200nM (Mohan et al., 2013). Here, suppression of catastrophe and rescue is enhanced for all values of α greater than our initial “small” dose ($\alpha = 7 \frac{\mu\text{m}}{\mu\text{M}\cdot\text{min}}$), thus in the context of our modeling framework, it is likely that MTAs and EBs do not work independently to promote MT dynamics at low MTA dose. Fig. 9 shows that similar results are found for increases in κ at the same EB concentration.

Next, we consider the case where EBs and MT stabilizing drugs do not interact independently from one another. In particular, we suggest that there is a *synergistic effect* so that MTAs enhance the action of the EBs. Recent studies suggest that such a synergistic effect exists, however this effect is not well understood. In this case, we propose that the MTAs work not only by increasing α (or κ), but also by strengthening the effect that the EBs have on the hydrolysis rate and the rescue propensity. Here, we rewrite the EB dependent hydrolysis rate (Eq. (20)) and the EB rescue rate (Eq. (21)) as

$$\gamma_{EB,M}^h(t) = \gamma^h + f_1(EB^b(t))(1 + f_3(M)) \quad (33)$$

and

$$\lambda_{EB,M}(t) = \lambda + f_2(EB^b(t))(1 + f_3(M)), \quad (34)$$

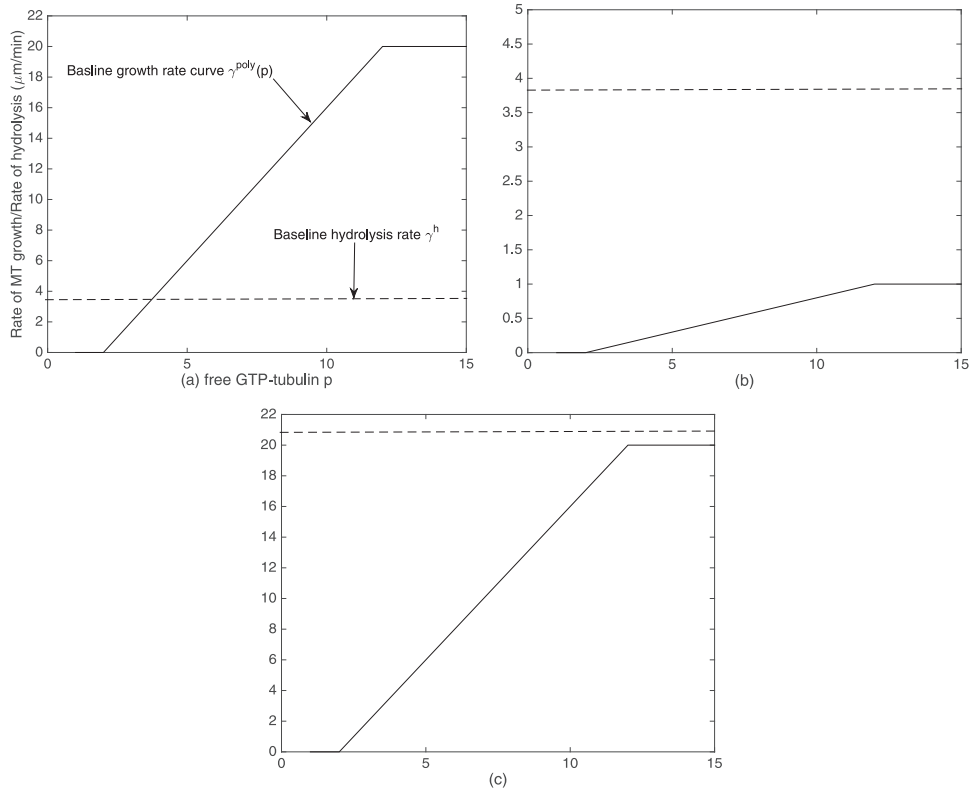


Fig. 6. Intersection between MT growth rate $\gamma^{\text{poly}}(p)$ and hydrolysis rate γ^h . (a) $\gamma^{\text{poly}}(p)$ and γ^h in our baseline case ($\alpha = 2$ and $\gamma^h = 3.8$). Here, the curves intersect and so MTs oscillate between periods of growth and shortening. (b) $\alpha = 0.1$ (see Fig. 5(a)) is small enough so that the curves do not intersect (MTs eventually depolymerize). (c) $\gamma^h = 21$ (see Fig. 5(c)) is high enough so that the curves do not intersect (MTs eventually depolymerize).

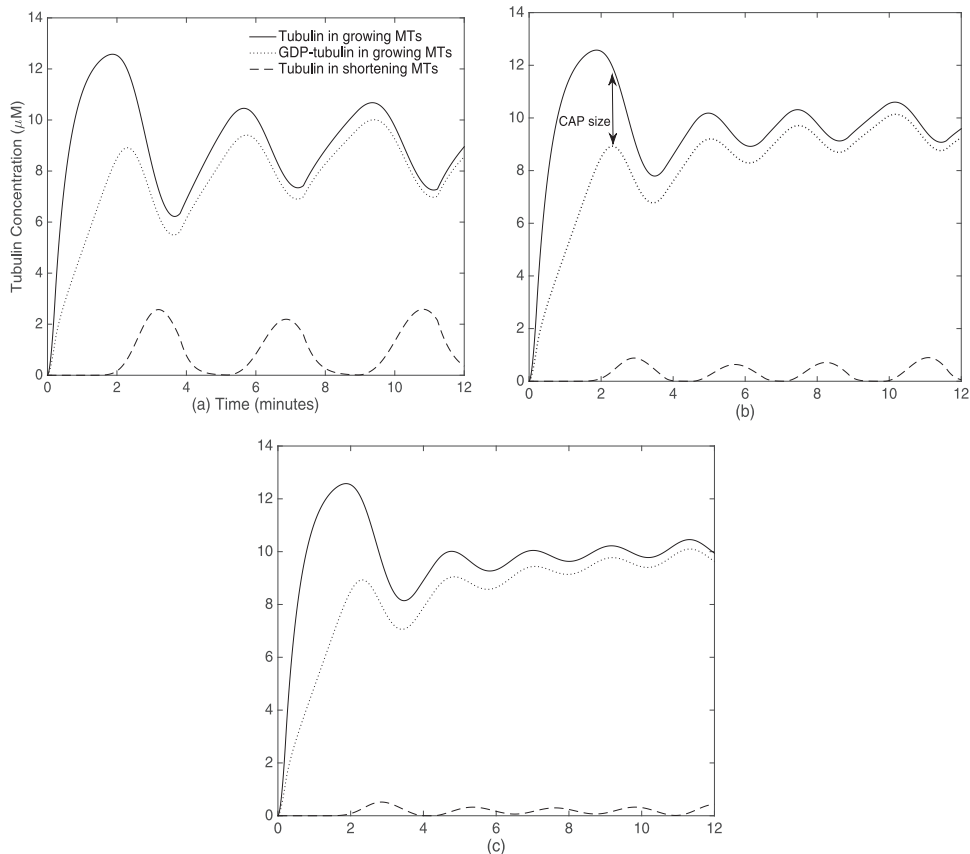


Fig. 7. Effect of varying the MT shortening rate δ . (a) Low $\delta = 5 \frac{\mu\text{m}}{\text{min}}$, (b) baseline $\delta = 15 \frac{\mu\text{m}}{\text{min}}$, and (c) high $\delta = 25 \frac{\mu\text{m}}{\text{min}}$.

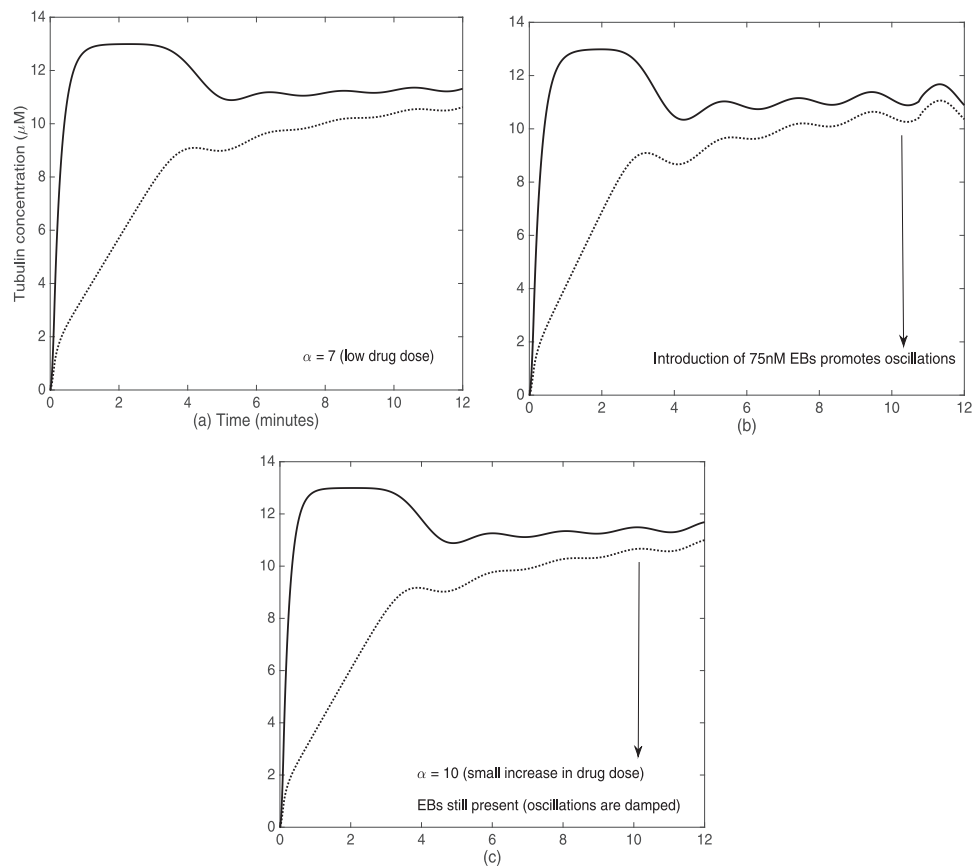


Fig. 8. MTAs act independently from EBs. (a) MTs are stabilized when $\alpha = 7 \frac{\mu\text{m}}{\mu\text{M}\cdot\text{min}}$, (b) 75 nM EBs induce oscillations (catastrophe and rescue) at $\alpha = 7 \frac{\mu\text{m}}{\mu\text{M}\cdot\text{min}}$, and (c) oscillations are damped at higher MTA dose ($\alpha = 10 \frac{\mu\text{m}}{\mu\text{M}\cdot\text{min}}$).

Table 7

Comparison of model output with experimental data (Pagano et al., 2012) in the presence of 75 nM of EB3.

	$\bar{\gamma}_{poly}$	f_c^{time}	f_c^{dist}
SI units	$\mu\text{m min}^{-1}$	min^{-1}	μm^{-1}
Experimental control (Pagano et al., 2012)	3.87 ± 1.00	1.72 ± 0.12	0.47 ± 0.03
1 nM paclitaxel	4.13 ± 1.47	2.10 ± 0.17	0.58 ± 0.04
10 nM paclitaxel	4.89 ± 1.56	2.62 ± 0.20	0.58 ± 0.045
100 nM paclitaxel	5.99 ± 1.54	2.96 ± 0.19	0.50 ± 0.033
Simulated "control" test 1	3.83	1.73	0.42
1 nM paclitaxel ($\kappa = 7$)	3.91	2.31	0.56
10 nM paclitaxel ($\kappa = 10$)	4.38	3.13	0.69
100 nM paclitaxel ($\kappa = 15$)	5.25	N/A	N/A
Simulated "control" test 2	3.83	1.73	0.42
1 nM paclitaxel ($\alpha = 7$)	3.94	1.80	0.42
10 nM paclitaxel ($\alpha = 8$)	5.17	3.01	0.52
100 nM paclitaxel ($\alpha = 10$)	9.75	N/A	N/A

so that in the absence of drugs we arrive at the original expressions. Here, M represents the drug dose, and $f_3(M)$ is some monotonically increasing function with respect to the drug dose. Here, we propose a linear response so that $f_3(M) = \gamma_M M$, where γ_M is a constant parameter used to describe the increased effect of the drug on hydrolysis and rescue.

Figs. 10 and 11 illustrate the results of increasing stabilizing MTA concentration up to 100 nM in the presence of 75 nM EBs (by increasing α and κ , respectively). In Table 7, we summarize the mean MT growth rates and catastrophe frequencies, and compare them to the results of Pagano et al. (2012). In the study of Pagano et al., the authors introduced paclitaxel into a system comprised of 15 μM tubulin and 75 nM EB3 (similar to our simula-

tions) and found increased catastrophe and rescue frequencies for increasing MTA dose (up to 100 nM paclitaxel). At MTA doses greater than 100 nM, catastrophes and rescues were suppressed. In the study of Mohan et al. (2013), the authors report similar increases in catastrophe and rescue frequency for paclitaxel doses up to 100 nM in systems comprised of 10 nM EB3. Qualitatively, our results are consistent with experiment. In particular, at low MTA doses, we find increases in time-based catastrophe, where catastrophe is suppressed at moderate MTA dose. It is important to note that, the values of κ and α which represent particular drug doses (see Table 7), have been selected to show the qualitative and quantitative features described in Figs. 10 and 11 and Table 7, respectively. However, when our model was simulated using different in-

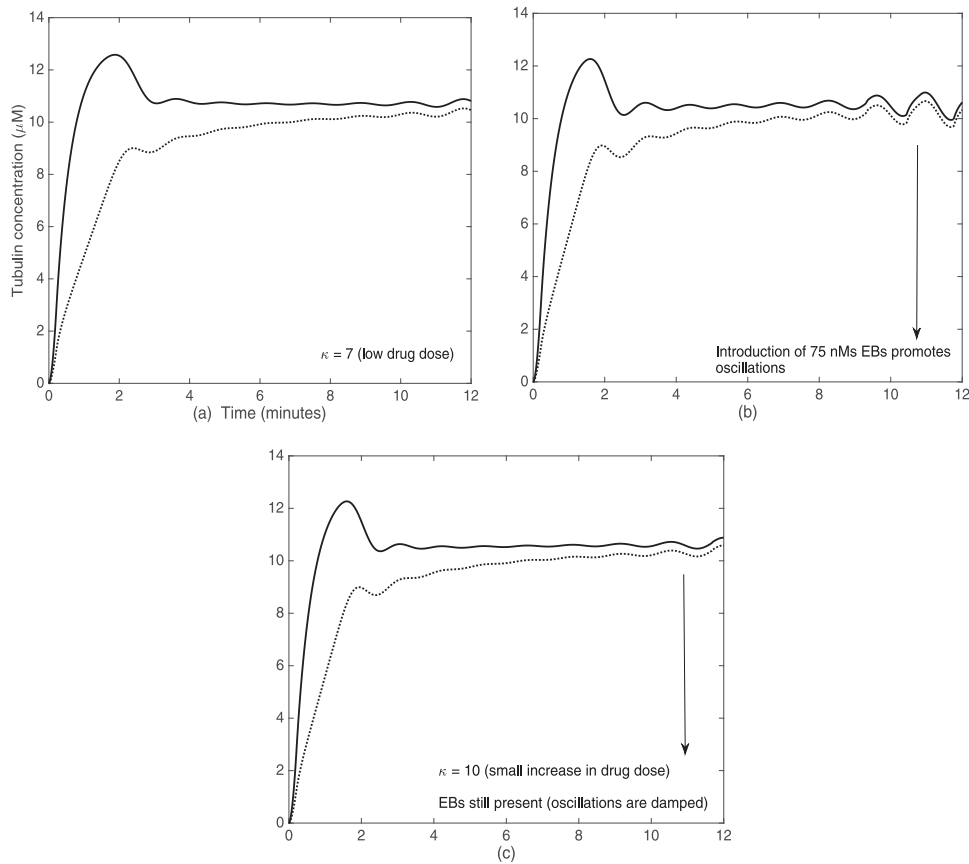


Fig. 9. MTAs act independently from EBs. (a) MTs are stabilized when $\kappa = 7 \frac{1}{\text{min}}$. (b) 75 nM EBs induce oscillations (catastrophe and rescue) at $\kappa = 7 \frac{1}{\text{min}}$, and (c) oscillations are damped at higher MTA dose ($\kappa = 10 \frac{1}{\text{min}}$).

creases for each parameter, we find qualitatively similar results (results not shown).

Experimental results summarized in Table 7 show that the frequencies of catastrophe and the MT growth rate increase for increasing MTA dose, up to 100 nM. Similar to the results of Pagano et al., simulation results illustrate an increase in the catastrophe frequencies and the MT growth rates up to 10 nM of the drug. Unlike the results of Pagano et al., catastrophe is suppressed for 100 nM of the drug (in experiment Pagano et al., 2012, MTs are stabilized at a higher MTA dose of approximately 200 nM).

To test robustness of the model, we have simulated our model for varying parameter γ_M ($0.1 < \gamma_M < 1.5$) and have found qualitatively similar results (results not shown). For different values of γ_M , and for different functional responses $f_3(M)$, it should be possible to make a better quantitative comparison to experiment, and this is the future goal of the project. Although our results are not quantitatively similar to experiment, our simulation results are qualitatively consistent to experiment (Pagano et al., 2012), and provide useful insight into the possible synergistic activity between MTAs and EBs.

5. Discussion

In this paper, we have developed a novel modeling approach to describe how MT dynamics are affected by EBs in an *in vitro* setting. Extending on the model of Hinow et al. (2009), we first define a new method for MT shortening (as opposed to the commonly used advection model), that can describe the very fast MT shortening events that characterize MT dynamic instability. This model takes into account both the MT shortening rate and the average MT shortening distance. The addition of the latter is important since,

when a MT undergoes a shortening event, it may only partially depolymerize (as evidenced in Pagano et al., 2012).

Further, we define novel mathematical expressions for the frequencies of catastrophe (time- and distance- based) using the method of characteristics. Such expressions are important as they can be used to compare simulation results with experiment. In the case of constant hydrolysis, we are able to define a relationship between the frequencies of catastrophe that is consistent with experiment. This result is significant, since it suggests that our definitions for catastrophe are biologically realistic with respect to this modeling framework.

By introducing a simple binding/unbinding model for EB kinetics, as well as expressions that describe changes to the hydrolysis and rescue rate in the presence of EBs, simulation results for MT dynamics are similar to those observed experimentally (Mohan et al., 2013; Vitre et al., 2008). In particular, we show that as the concentration of EBs increases, so too does the MT growth rate and the time-based catastrophe frequency. Also, simulation results show that there is less variation in the distance-based catastrophe for increasing EB concentration, a result that is also consistent with experiment. Further, we find that the time-based catastrophe frequency saturates in value for high EB concentrations, a result that has been verified by Mohan et al. (2013). To verify that this saturating effect is not just a result of the control parameter sets selected (Tables 3 and 4), we show that the same (qualitative) result holds true for a variety of different parameter sets (see Appendix A).

In addition to describing the effects of EBs on MT dynamics, we also describe how increases and decreases in particular model parameters alter the qualitative behavior of solution curves. Specifically, we find that increases in α (the MT growth parameter) and

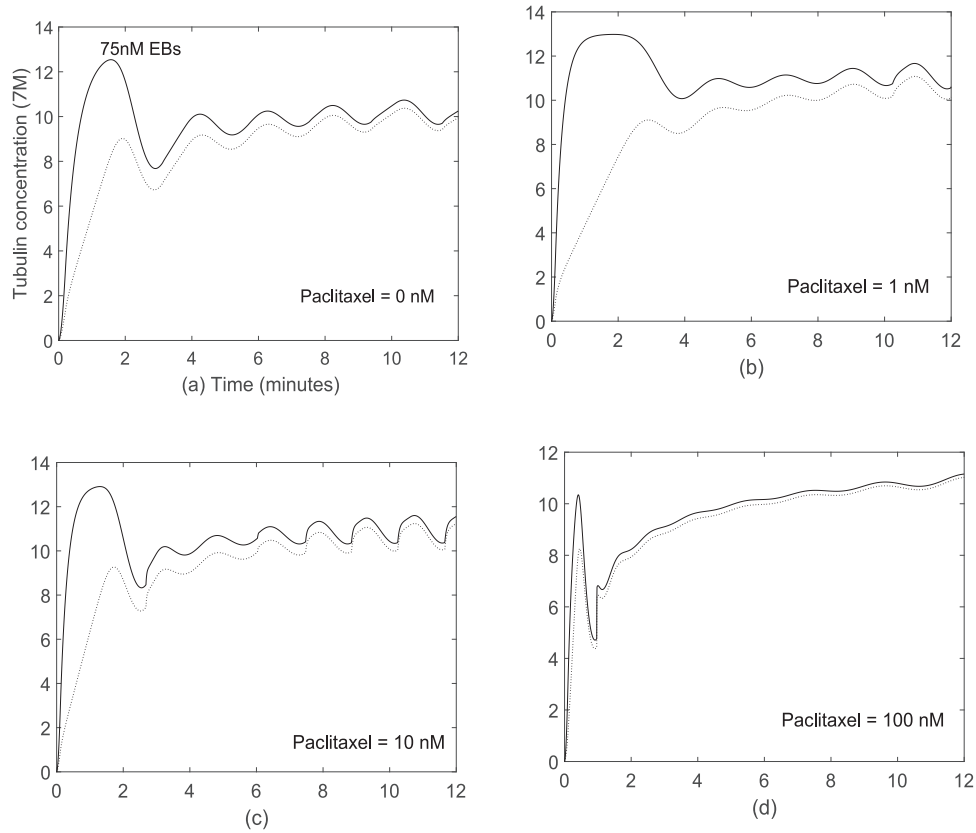


Fig. 10. MTAs enhance effect of EBs. Here, we set the parameter $\gamma_M = 0.5 \text{ nM}^{-1}$. (a) MTs in presence of 75 nM EBs and no drugs ($\alpha = 2 \frac{\mu\text{m}}{\mu\text{M}\cdot\text{min}}$, $M = 0 \text{ nM}$). (b) MTs in presence of 75 nM EBs and 1 nM paclitaxel ($\alpha = 7 \frac{\mu\text{m}}{\mu\text{M}\cdot\text{min}}$, $M = 1$). (c) MTs in presence of 75 nM EBs and 10 nM paclitaxel ($\alpha = 8 \frac{\mu\text{m}}{\mu\text{M}\cdot\text{min}}$, $M = 10$). (d) MTs in presence of 75 nM EBs and 100 nM paclitaxel ($\alpha = 10 \frac{\mu\text{m}}{\mu\text{M}\cdot\text{min}}$, $M = 100$).

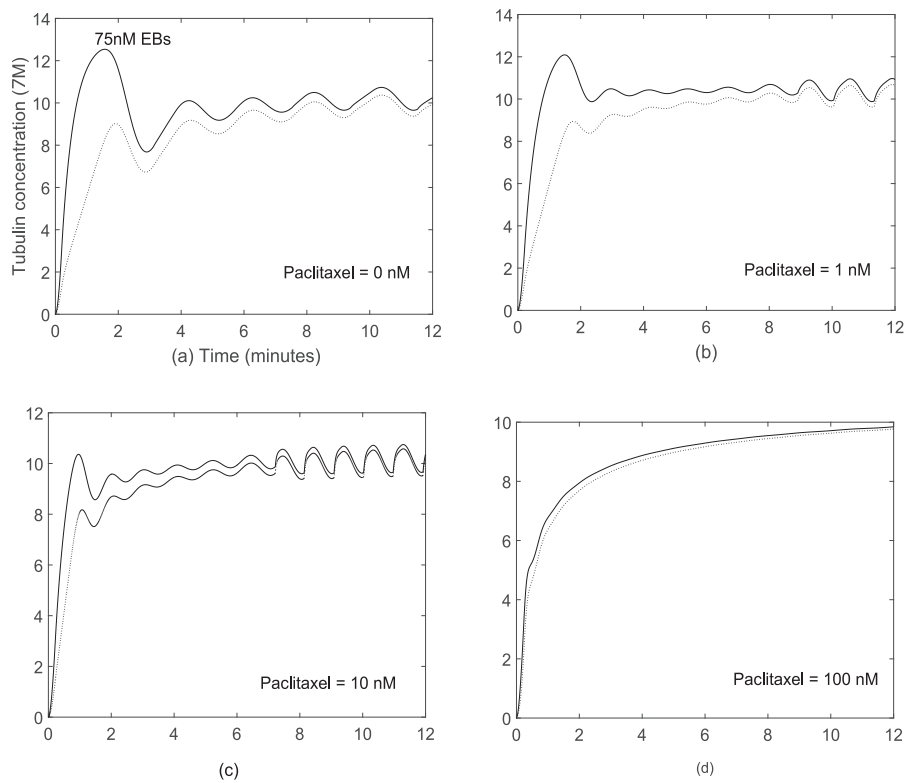


Fig. 11. MTAs enhance effect of EBs. Here, we set the parameter $\gamma_M = 0.3 \text{ nM}^{-1}$. (a) MTs in presence of 75 nM EBs and no drugs ($\kappa = 1 \frac{1}{\text{min}}$, $M = 0 \text{ nM}$). (b) MTs in presence of 75 nM EBs and 1 nM paclitaxel ($\kappa = 7 \frac{1}{\text{min}}$, $M = 1$). (c) MTs in presence of 75 nM EBs and 10 nM paclitaxel ($\kappa = 10 \frac{1}{\text{min}}$, $M = 10$). (d) MTs in presence of 75 nM EBs and 100 nM paclitaxel ($\kappa = 15 \frac{1}{\text{min}}$, $M = 100$).

κ (the GDP/GTP exchange rate) both act to promote MT polymerization and stabilization. This result leads us to an assumption that MT stabilizing drugs, like drugs from the paclitaxel family, work by increasing at least one of these rates. From a biological perspective, this result makes sense, as increases in both of these parameters should promote MT polymerization (MT growth), just as a stabilizing drug would do. It is important to note here that, in order for MTs to be completely stabilized, the MT growth rate must be larger than or equal to the hydrolysis rate γ^h (after some time). In our system, for the examples shown in Figs. 5(a) and (b) when κ and α are large, the growth rate is initially larger than the hydrolysis rate. However, the hydrolysis rate eventually becomes smaller than the growth rate and the cap shortens (result not shown in this figure). If we simulate the behavior of solutions for longer periods of time, the cap size will eventually reach zero, and MTs will shorten for some period of time, but will eventually start oscillating again. However, for the time periods we have shown, MTs remain stabilized. Further, these time periods correspond to realistic experimental time frames.

In vitro, in the absence of EBs, stabilizing MTAs are effective at both low and high doses. That is, they work to stabilize MTs by suppressing MT dynamic instability. However, when EBs are also present, MT dynamic instability is promoted and catastrophe frequencies increase in a drug dependent way. However, this effect is only found at low MTA dose. When the MTA dose is high enough, MTs are stabilized, just as in the case when there are no EBs present. To examine how the combination of EBs and MTAs might work to promote dynamic instability, we consider two cases: either EBs and MTAs work independently from one another, or they work together in some synergistic way. In the case that EBs and MTAs work independently, we find that increases in stabilizing MTA concentration works to damp oscillations in the polymer solution curves, thus suppressing rather than promoting MT dynamics. Thus, in the context of this modeling framework, it is likely that MTAs and EBs do not work independently from one another to promote MT dynamics at low MTA doses. To gain insight into how EBs might work synergistically with MTAs, we consider the case where the addition of MTAs enhance the effect of the EBs. Here, we consider simple functional forms (33) and (34), that describe how MTAs enhance EB action, and find results that are qualitatively consistent with experiment. That is, for increasing stabilizing MTA concentration, MT dynamic instability is promoted (as shown by increases in the oscillations of polymer solution curves and increases in the catastrophe frequencies). Further, we show that for high enough MTA dose, MT dynamics are suppressed (i.e., there is no MT catastrophe). Both these results are consistent with experiment (Pagano et al., 2012). Again, it should be noted that we have only considered one possible mechanism for synergy. A more detailed analysis into appropriate synergistic forms for the equations (33) and (34) should be completed, to obtain more biologically meaningful results.

In future studies, it would be interesting to consider a spatial model for EBs, since in both *in vivo* and *in vitro* settings, EB comets have been observed. In particular, it is not true that EBs distribute themselves evenly along the entirety of the GTP cap region, as is assumed in this model. Rather, EBs bind and unbind in such a way that they form growing and shortening comet-like structures (Maurer et al., 2014). Also, it is known that the action of EBs on MTs is different *in vivo* (Berges et al., 2014) than *in vitro*. Therefore, it will be important to investigate the action of EBs in an *in vivo* setting as well. Reasons for the differences in EB action *in vivo* might be explained by the underlying processes that regulate EB protein binding, including post-translational modifications such as deuterionisation/retyrosination (Rovini et al., 2013), acetylation, and/or phosphorylation (Grand et al., 2014). Finally, in addition to considering the action of stabilizing MTAs on MT dynamics

in the presence of EBs, it will be important to study the action of destabilizing drugs in such systems. This is because similar synergistic effects have been reported between EBs and destabilizing MTAs from the vinca alkaloid family (Mohan et al., 2013) and/or the colchicine family (Berges et al., 2016).

Another important extension will be to consider a spatially dependent free-tubulin concentration, where diffusion of tubulin plays a role. Along with spatially dependent tubulin concentrations, it will be interesting to consider a boundary, representative of a cell cortex. This will restrict MT length, and allow us to consider a *paused state* for MTs. MTs have been shown to pause for some time after reaching the boundary before undergoing a catastrophe, and such pausing has been shown to impact MT dynamics (Ebbinghaus and Santen, 2011).

The results of this study give new insight into the action of EBs and MTAs on MT dynamics. Through development and simulation of a mathematical model, we describe how EBs can work to alter MT dynamics in an *in vitro* setting. Further, by developing biologically realistic mathematical expressions for the time- and distance-based catastrophe frequencies, we were able to show that our simulation results were consistent with experiment. In addition to describing how EBs alter MT dynamics, we describe a potential mechanism to explain how stabilizing MTAs can work synergistically with EBs to promote MT dynamics at low MTA dose. In future studies it will be important to test other types of synergistic relationships, other than those described in this paper, to obtain results that are consistent both quantitatively and qualitatively with experiment.

Acknowledgments

This work has been carried out thanks to (1) the support of the A*MIDEX project (n° ANR-11-IDEX-0001-02) funded by the “Investissements d’Avenir” French Government program, managed by the French National Research Agency (ANR) and (2) the support of INSERM/ITMO Cancer (Plan Cancer 2014–2019) “Domaine de la Physique, des mathématiques ou des sciences de l’ingénieur appliqués au Cancer” n° PC201418 and PC201419. D.W. was supported by the programs cited above through post-doc funding, and F.H. was partially supported by the programs cited above.

Appendix A

Here, we show that the trends recorded in Table 6 hold true for a variety of model parameters. In particular, for increasing EB concentration, the mean growth rate $\bar{\gamma}^{poly}$ increases, the decoration time DT decreases, the time-based catastrophe f_c^{time} increases (sometimes saturating at high EB concentrations), and the distance-based catastrophe f_c^{dist} increases (although only slightly

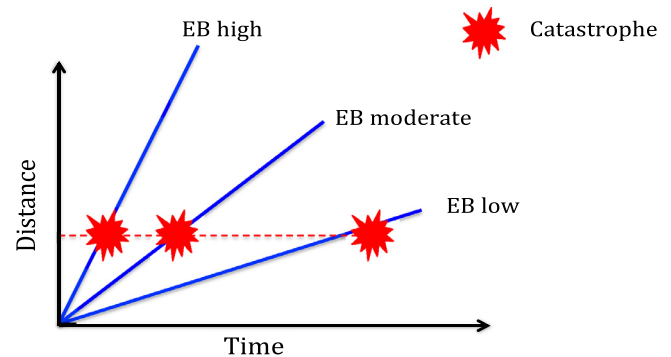


Fig. A.1. Schematic to describe the saturating effect of EBs on the time-based catastrophe frequency.

Table A.1
Variation of model parameters from baseline. Parameters that are varied are highlighted in bold.

Parameter SI units	p_c μM	p_s μM	α $\frac{\mu\text{m}}{\text{min}\cdot\mu\text{M}}$	γ^h $\frac{\mu\text{m}}{\text{min}}$	δ $\frac{\mu\text{m}}{\text{min}}$	x_0 μm	SD of x_0 μm	λ $\frac{\mu\text{m}}{\text{min}}$	μ $\frac{1}{\text{M}\cdot\text{min}}$	n	κ $\frac{1}{\text{min}}$
Control test	2	12	2	3.8	15	4	1	0.136	59×10^{-4}	2	1
test 1	2	12	1	3.8	15	4	1	0.136	59×10^{-4}	2	1
test 2	2	12	3	3.8	15	4	1	0.136	59×10^{-4}	2	1
test 3	2	12	4	3.8	15	4	1	0.136	59×10^{-4}	2	1
test 4	2	12	2	3	15	4	1	0.136	59×10^{-4}	2	1
test 5	2	12	2	5	15	4	1	0.136	59×10^{-4}	2	1
test 6	2	12	2	3.8	10	4	1	0.136	59×10^{-4}	2	1
test 7	2	12	2	3.8	20	4	1	0.136	59×10^{-4}	2	1
test 8	2	12	2	3.8	15	4	1	0.136	59×10^{-4}	2	0.5
test 9	2	12	4	4.5	15	4	1	0.136	59×10^{-4}	2	1
test 10	2	12	6	6.5	20	4	1	0.136	59×10^{-4}	2	1

Table A.2
Increase in catastrophe frequency and growth rate for increasing EB concentration. EB model parameters are outlined in Table 3.

EB concentration (nM)	0	25	50	75	100	125
Control test						
$\tilde{\gamma}^{poly} (\frac{\mu\text{m}}{\text{min}})$	3.54	3.67	3.76	3.83	3.88	3.94
$f_c^{time} (\frac{1}{\text{min}})$	1.545	1.595	1.686	1.728	1.764	1.730
$f_c^{dist} (\frac{1}{\mu\text{m}})$	0.4077	0.4050	0.4145	0.4164	0.4099	0.3912
DT (sec)	10.12	9.07	8.27	7.62	7.02	6.49
test 1						
$\tilde{\gamma}^{poly} (\frac{\mu\text{m}}{\text{min}})$	3.68	3.75	3.79	3.84	3.90	3.95
$f_c^{time} (\frac{1}{\text{min}})$	1.10	1.08	1.26	1.32	1.46	1.45
$f_c^{dist} (\frac{1}{\mu\text{m}})$	0.2950	0.2754	0.3105	0.3166	0.3492	0.3392
DT (sec)	6.82	6.10	5.49	4.97	4.53	4.17
test 2						
$\tilde{\gamma}^{poly} (\frac{\mu\text{m}}{\text{min}})$	3.52	3.62	3.70	3.80	3.93	4.04
$f_c^{time} (\frac{1}{\text{min}})$	1.06	1.28	1.77	2.00	2.07	2.01
$f_c^{dist} (\frac{1}{\mu\text{m}})$	0.2788	0.3230	0.4320	0.4767	0.4779	0.4539
DT (sec)	12.00	10.65	9.52	8.51	7.70	7.07
test 3						
$\tilde{\gamma}^{poly} (\frac{\mu\text{m}}{\text{min}})$	3.44	3.57	3.66	3.80	3.94	4.07
$f_c^{time} (\frac{1}{\text{min}})$	0.17	1.24	1.36	1.76	1.81	1.82
$f_c^{dist} (\frac{1}{\mu\text{m}})$	0.0442	0.2524	0.2536	0.3197	0.3201	0.3138
DT (sec)	14.57	12.86	11.49	10.14	9.10	8.31
test 4						
$\tilde{\gamma}^{poly} (\frac{\mu\text{m}}{\text{min}})$	2.72	2.88	3.01	3.10	3.19	3.26
$f_c^{time} (\frac{1}{\text{min}})$	0.1735	0.4614	1.11	1.02	1.15	1.22
$f_c^{dist} (\frac{1}{\mu\text{m}})$	0.0582	0.1421	0.3339	0.2946	0.3205	0.3289
DT (sec)	15.79	13.28	11.55	10.31	9.31	8.56
test 5						
$\tilde{\gamma}^{poly} (\frac{\mu\text{m}}{\text{min}})$	3.52	3.75	3.79	3.84	3.90	3.95
$f_c^{time} (\frac{1}{\text{min}})$	1.06	1.08	1.26	1.32	1.46	1.45
$f_c^{dist} (\frac{1}{\mu\text{m}})$	0.2788	0.2754	0.3105	0.3166	0.3492	0.3392
DT (sec)	12.00	6.10	5.49	4.97	4.53	4.17

Table A.3
Increase in catastrophe frequency and growth rate for increasing EB concentration. EB model parameters are outlined in Table 3 in the main text.

EB concentration (nM)	0	25	50	75	100	125
Control test						
$\tilde{\gamma}^{poly} (\frac{\mu\text{m}}{\text{min}})$	3.54	3.67	3.76	3.83	3.88	3.94
$f_c^{time} (\frac{1}{\text{min}})$	1.545	1.595	1.686	1.728	1.764	1.730
$f_c^{dist} (\frac{1}{\mu\text{m}})$	0.4077	0.4050	0.4145	0.4164	0.4099	0.3912
DT (sec)	10.12	9.07	8.27	7.62	7.02	6.49
test 6						
$\tilde{\gamma}^{poly} (\frac{\mu\text{m}}{\text{min}})$	3.63	3.62	3.75	3.82	3.86	3.91
$f_c^{time} (\frac{1}{\text{min}})$	1.30	1.75	1.88	1.84	1.85	1.88
$f_c^{dist} (\frac{1}{\mu\text{m}})$	0.2715	0.3443	0.3558	0.3403	0.3327	0.3284
DT (sec)	10.89	9.25	8.15	7.36	6.72	6.09
test 7						
$\tilde{\gamma}^{poly} (\frac{\mu\text{m}}{\text{min}})$	3.56	3.65	3.73	3.80	3.87	3.94
$f_c^{time} (\frac{1}{\text{min}})$	1.02	1.49	1.52	1.46	1.61	1.50
$f_c^{dist} (\frac{1}{\mu\text{m}})$	0.2095	0.2920	0.2842	0.2696	0.2855	0.2623
DT (sec)	9.86	8.95	8.20	7.56	7.01	6.51
test 8						
$\tilde{\gamma}^{poly} (\frac{\mu\text{m}}{\text{min}})$	3.70	3.77	3.84	3.92	4.00	4.07
$f_c^{time} (\frac{1}{\text{min}})$	0.48	0.49	0.51	0.51	0.51	0.8
$f_c^{dist} (\frac{1}{\mu\text{m}})$	0.1150	0.1107	0.1087	0.1040	0.1004	0.1513
DT (sec)	10.79	10.01	9.35	8.79	8.25	7.66
test 9						
$\tilde{\gamma}^{poly} (\frac{\mu\text{m}}{\text{min}})$	4.84	4.80	4.80	4.89	5.00	5.06
$f_c^{time} (\frac{1}{\text{min}})$	0.75	1.07	1.25	1.49	1.62	1.65
$f_c^{dist} (\frac{1}{\mu\text{m}})$	0.1503	0.2074	0.2354	0.2791	0.2975	0.2980
DT (sec)	6.93	6.11	5.39	4.80	4.35	4.05
test 10						
$\tilde{\gamma}^{poly} (\frac{\mu\text{m}}{\text{min}})$	6.11	6.12	6.28	6.29	N/A	
$f_c^{time} (\frac{1}{\text{min}})$	1.72	2.11	2.63	2.34	N/A	
$f_c^{dist} (\frac{1}{\mu\text{m}})$	0.264	0.316	0.346	0.340	N/A	
DT (sec)	6.88	5.80	5.30	4.91	N/A	

in many cases). Table A.1 outlines each test we complete, and Tables A.2 and A.3 give the results for each test. More specifically, each table lists the mean growth rate $\tilde{\gamma}^{poly}$, the time-based catastrophe f_c^{time} , the distance-based catastrophe f_c^{dist} , and the decoration time DT for increasing EB concentration.

A schematic to describe the trend we see in these tables, as well as the trend observed in the original Table 6 is illustrated in Fig. A.1. The figure gives the time before a catastrophe VS the length of a MT before a catastrophe event.

For increasing EB concentration, the slope of the velocity curve increases. The red bullets correspond to catastrophe events. If we assume that the distance before a catastrophe is approximately constant, the time before a catastrophe occurs decreases for increasing EB concentration (hence the time-based catastrophe frequency increases). If the EB concentration is increased further, the

time before a catastrophe changes very little (i.e., the catastrophe events get very close together, explaining the saturation effect).

Supplementary material

Supplementary material associated with this article can be found, in the online version, at [10.1016/j.jtbi.2017.06.014](https://doi.org/10.1016/j.jtbi.2017.06.014).

References

Barlukova, A., White, D., Henry, G., Honore, S., Hubert, F., 2017. Mathematical modeling of microtubule dynamic instability: new insight into the link between GTP-hydrolysis and microtubule aging. ESAIM Mathematical Modelling and Numerical Analysis.

- Berges, R., Baeza-Kallee, N., Tabouret, E., Chinot, O., Petit, M., Kruczynski, A., Figarella-Branger, D., Honore, S., Braguer, D., 2014. End-binding 1 protein overexpression correlates with glioblastoma progression and sensitizes to vinca-alkaloids in vitro and in vivo. *Oncotarget* 5 (24), 1–19.
- Berges, R., Tchoghandjian, A., Honore, S., Esteve, M., Figarella-Branger, D., Bachmann, F., Lane, H., Braguer, D., 2016. The novel tubulin-binding checkpoint activator bal101553 inhibits eb1-dependent migration and invasion and promotes differentiation of glioblastoma stem-like cells. *Mol. Cancer Ther.* 15 (11), 2740–2749.
- Chen, Y., Hill, T., 1985. Monte Carlo study of the GTP cap in a five-start helix model of a microtubule. *PNAS* 82, 1131–1135.
- Desai, A., Mitchison, T., 1997. Microtubule polymerization dynamics. *Annu. Rev. Cell Dev. Biol.* 13, 83–117.
- Dogterom, M., Leibler, S., 1993. Physical aspects of the growth and regulation of microtubule structures. *Phys. Rev. Lett.* 70, 1347–1350.
- Ebbinghaus, M., Santen, L., 2011. Theoretical modeling of aging effects in microtubule dynamics. *Theor. Model. Aging Effects Microtubule Dyn.* 100, 832–838.
- Etienne-Manneville, S., 2013. Microtubules in cell migration. *Cell Dev. Biol.* 29, 471–499.
- Flyvbjerg, H., Holy, T., Leibler, S., 1994. A model for caps and catastrophes. *Phys. Rev. Lett.* 73, 2372–2375.
- Flyvbjerg, H., Holy, T., Leibler, S., 1996. Microtubule dynamics: caps, catastrophes, and coupled hydrolysis. *Phys. Rev. Lett.* 54, 5538–5560.
- Gardner, M., Zanic, M., Gell, C., Bormuth, V., Howard, J., 2011. The depolymerizing kinesins kip3 (kinesin-8) and mcak (kinesin-13) are catastrophe factors that destabilize microtubules by different mechanisms. *Nat. Cell Biol.* 147 (5), 1092–1103.
- Grand, M.L., Rovini, A., Bourgarel-Rey, V., Honore, S., Bstonero, S., Braguer, D., Carre, M., 2014. Ros-mediated eb1 phosphorylation through akt/gsk3 β pathway: implication in cancer cell response to microtubule targeting agents. *Oncotarget* 5 (10), 3408–3423.
- Hinow, P., Rezaia, V., Lopus, M., Jordan, M., Tuszynski, J., 2011. Modeling the effects of drug binding on the dynamic instability of microtubules. *Phys. Biol.* 8 (5), doi:10.1088/1478-3975/8/5/056004.
- Hinow, P., Rezaia, V., Tuszynski, J., 2009. Continuous model for microtubule dynamics with catastrophe, rescue, and nucleation processes. *Phys. Rev.* 80. doi:10.1103/PhysRevE.80.031904.
- Honore, S., 2015. Personal communication.
- Jiang, K., Akhmanova, A., 2011. Microtubule tip-interacting proteins: a view from both ends. *Curr. Opin. Cell Biol.* 23, 94–101.
- Lacroix, B., Maddox, A., 2014. Microtubule dynamics followed through cell differentiation and tissue biogenesis in *c. elegans*. *Worm* 3 (3). doi:10.4161/21624046.2014.967611.
- Lodish, H., Berk, A., Zipursky, S.L., Matsudaira, P., Baltimore, D., Darnell, J., 2000. *Molecular Cell Biology*, 4 W. H. Freeman and Company, New York.
- Martin, S., Schilstra, M., Bayley, P., 1993. Dynamic instability of microtubules: monte carlo simulation and application to different types of microtubule lattice. *Biophys. J.* 65, 578–596.
- Maurer, S., Cade, N., Bohner, G., Gustafsson, N., Boutant, E., Surrey, T., 2014. Eb1 accelerates two conformational transitions important for microtubule maturation and dynamics. *Curr. Biol.* 24, 372–384.
- Maurer, S., Fourniol, F., Bohner, G., Moores, C., Surrey, T., 2012. Ebs recognize a nucleotide-dependent structural cap at growing microtubule ends. *Cell* 149, 371–382.
- Mishra, P., Kunwar, A., Mukherji, S., Chowdhury, D., 2005. Dynamic instability of microtubules: effect of catastrophe-suppressing drugs. *Phys. Rev. Lett.* 72. DOI:051914
- Mitchison, T., Kirschner, M., 1984. Dynamic instability of microtubule growth. *Nature* 312, 237–242.
- Mohan, R., Katrukha, E., Doodhi, H., Smal, I., Meijering, E., Kapitein, L., Steinmetz, M., Akhmanova, A., 2013. End-binding proteins sensitize microtubules to the action of microtubule-targeting agents. *PNAS* doi:10.1073/pnas.1300395110.
- Mukhtar, E., Adhami, V.M., Mukhtar, H., 2014. Targeting microtubules by natural agents for cancer therapy. *Mol. Cancer Ther.* 93, 275–284.
- Pagano, A., Honore, S., Mohan, R., Berges, R., Akhmanova, A., 2012. Etoposide b inhibits migration of glioblastoma cells by inducing microtubule catastrophes and affecting eb1 accumulation at microtubule plus ends. *Biochem. Pharmacol.* 84, 432–443.
- Rovini, A., Gauthier, G., Berges, R., Kruczynski, A., Braguerr, D., 2013. Antimigratory effect of vinflunine in endothelial and glioblastoma cells is associated with changes in eb1 c-terminal detyrosinated/tyrosinated status. *PLoS ONE* 8. doi:10.1371/journal.pone.0065694.
- Seetapun, D., Castle, B., McIntyre, A., Tran, P., Odde, D., 2012. Estimating the microtubule gtp cap size in vivo. *Nat. Cell Biol.* 22 (8), 16811687.
- Sept, D., Limbach, H., Bolterauer, H., Tuszynski, J., 1999. A chemical kinetics model for microtubule oscillations. *J. Theor. Biol.* 197, 77–88.
- Vitre, B., Coquelle, F., Heichette, C., Garnier, C., Chretien, D., Arnal, I., 2008. Eb1 regulates microtubule dynamics and tubulin sheet closure in vitro. *Nat. Cell Biol.* 10, 415–421.
- Wade, R., 2009. On and around microtubules: an overview. *Mol. Biotechnol.* 43, 177–191.
- Walker, R., O'Brien, E., Pryer, N., Soboeiro, M., Voter, W., Erickson, H., Salmon, E., 1988. Dynamic instability of individual microtubules analyzed by video light microscopy: Rate constants and transition frequencies. *J. Cell Biol.* 107, 1437–1448.
- Wieczorek, M., Bechstedt, S., Chaaban, S., Brouhard, G., 2015. Microtubule-associated proteins control the kinetics of microtubule nucleation. *Nat. Cell Biol.* 17, 907–916.
- Wollman, R., Cytrynbaum, E., Jones, T., Meyer, T., Scholey, J., Mogilner, A., 2005. Efficient chromosome capture requires a bias in the search-and-capture process during mitotic-spindle assembly. *Curr. Biol.* 15. doi:10.1016/j.cub.2005.03.019.
- Zanic, M., Stear, J., Hyman, A., Howard, J., 2009. Eb1 recognizes the nucleotide state of tubulin in the microtubule lattice. *PLoS ONE* 10. e7585–e7585
- Zauderer, E., 2006. *Partial Differential Equations of Applied Mathematics*, 3 John Wiley and Sons, Inc. New Jersey.
- Zhou, J., Giannakakou, P., 2005. Targeting microtubules for cancer chemotherapy. *Current Medical Chemistry* 5, 65–71.